

Efficient and Accurate Optimal Transport with Mirror Descent and Conjugate Gradients

Mete Kemertas^{1,2*} Allan D. Jepson¹ Amir-massoud Farahmand^{2,1}

¹Department of Computer Science, University of Toronto

²Vector Institute

Abstract

We design a novel algorithm for optimal transport by drawing from the entropic optimal transport, mirror descent and conjugate gradients literatures. Our algorithm is able to compute optimal transport costs with arbitrary accuracy without running into numerical stability issues. The algorithm is implemented efficiently on GPUs and is shown empirically to converge more quickly than traditional algorithms such as Sinkhorn’s Algorithm both in terms of number of iterations and wall-clock time in many cases. We pay particular attention to the entropy of marginal distributions and show that high entropy marginals make for harder optimal transport problems, for which our algorithm is a good fit. We provide a careful ablation analysis with respect to algorithm and problem parameters, and present benchmarking over the MNIST dataset. The results suggest that our algorithm can be a useful addition to the practitioner’s optimal transport toolkit. Our code is open-sourced at <https://github.com/adaptive-agents-lab/MDOT-PNCG>.

1 Introduction

Efficient and accurate computation of optimal transport (OT) distances is a central problem in machine learning with notable applications in generative modelling (Gulrajani et al., 2017), reinforcement learning (Ferns et al., 2004; Dadashi et al., 2021) and neural architecture search (Kandasamy et al., 2018) among many others. Whenever one requires a metric-aware statistical distance given an event space equipped with a metric, OT distances such as the Wasserstein metric provide an intuitive recipe with desirable theoretical properties. While significant progress was made on the efficiency front with the introduction of Sinkhorn’s Algorithm (SA) to the world of GPUs (Sinkhorn & Knopp, 1967; Sinkhorn, 1967; Cuturi, 2013), this efficiency comes at the cost of a poor trade-off between accuracy and numerical stability. Issues posed by this trade-off are especially apparent when dealing with high entropy distributions, which are given particular attention in this work. While various sophisticated new algorithms have favourable theoretical convergence properties over SA, they are rarely as GPU-friendly (or parallelizable) and easy-to-implement such that SA still remains the baseline solution in practice (Flamary et al., 2021; Lin et al., 2022). In this work, we set out to design a flexible new algorithm that shares similar characteristics (e.g., parallelizability, practical efficiency) to SA, but can compute arbitrarily accurate solutions rapidly without sacrificing numerical stability.

Contributions. Our first contribution is to formally define and study the generalization of SA as a mirror descent procedure with approximate Bregman projections. We empirically show that with a heuristic warm-start of the optimization problem encountered over consecutive Bregman projection problems in mirror descent, one can efficiently approximate OT distances with arbitrary accuracy. Furthermore, we empirically show that at lower accuracy levels, where SA can also be employed without running into numerical instability issues, this algorithm can reach the same level of accuracy in fewer iterations, often with better wall-clock time on GPUs. Our second contribution is a new Bregman projection algorithm for OT. The approach introduces a novel instantiation of the conjugate gradients method suited to the Bregman projection problems encountered in the generalized mirror

*Correspondence to: kemertas@cs.toronto.edu

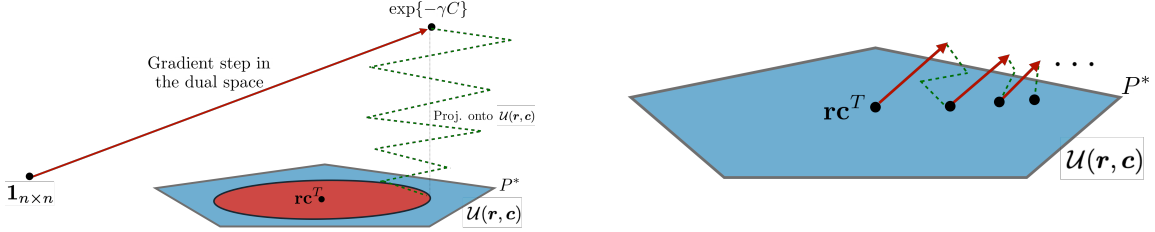


Figure 1: Depiction of SA (Cuturi, 2013) (Left) and mirror descent (Right) for the OT problem.

descent view of SA. In practice, the algorithm finds approximate projections of infeasible matrices onto the transportation polytope in up to $10\times$ fewer iterations than SA and is up to $5\times$ faster in terms of wall-clock time on a GPU. Combined with the mirror descent approach, they make for a strong contender to the practitioner’s go-to algorithm especially when high accuracy solutions are desired.

2 Background

Here, we outline our notation and provide the necessary background for the mirror descent (MD) and conjugate gradients components of our approach (see Appx. A for an extended version of this section and Appx. D for a detailed discussion of related work).

2.1 Notation and Definitions

We are concerned in this work with discrete OT, where the event space \mathcal{X} is finite with n elements. $\Delta_n \subset \mathbb{R}_{\geq 0}^n$ denotes the $(n-1)$ -probability simplex. We denote the row sum of a matrix $P \in \mathbb{R}^{n \times n}$ as $\mathbf{r}(P) = P\mathbf{1}_n$ and similarly the column sum by $\mathbf{c}(P) = P^\top \mathbf{1}_n$. The transportation polytope defined by target marginals $\mathbf{r}, \mathbf{c} \in \Delta_n$ is written as $\mathcal{U}(\mathbf{r}, \mathbf{c}) = \{P \in \mathbb{R}_{\geq 0}^{n \times n} \mid \mathbf{r}(P) = \mathbf{r}, \mathbf{c}(P) = \mathbf{c}\}$. Throughout, we assume all entries of \mathbf{r}, \mathbf{c} are positive. Operations \exp , \log and division over vectors or matrices indicate element-wise operations. For elementwise multiplication, we use the symbol \odot . Vectors in \mathbb{R}^n are taken to be column vectors. Matrix and vector inner products alike are given by $\langle \cdot, \cdot \rangle$. An $n \times n$ diagonal matrix with $\mathbf{x} \in \mathbb{R}^n$ along the diagonal is written as $\mathbf{D}(\mathbf{x})$.

2.2 Optimal Transport

Given a cost matrix $C \in [0, 1]^{n \times n}$, where C_{ij} is the cost of transportation between $\mathbf{x}_i, \mathbf{x}_j \in \mathcal{X}$, and $\mathbf{r}, \mathbf{c} \in \Delta_n$, we study the optimal transport problem given by the following linear program:

$$\underset{P \in \mathcal{U}(\mathbf{r}, \mathbf{c})}{\text{minimize}} \quad \langle P, C \rangle. \quad (1)$$

Entropic regularization of (1) is often used for efficient computation on GPUs (Cuturi, 2013):

$$\underset{P \in \mathcal{U}(\mathbf{r}, \mathbf{c})}{\text{minimize}} \quad \langle P, C \rangle - \frac{1}{\gamma} H(P), \quad (2)$$

where $\gamma > 0$ and $H(P) = -\sum_{ij} P_{ij} \log P_{ij}$ is the Shannon entropy of the joint distribution P . The Lagrangian of (2) is strictly convex in P so that a unique solution with respect to P exists:

$$P(\mathbf{u}, \mathbf{v})_{ij} = \exp\{u_i + v_j - \gamma C_{ij}\}. \quad (3)$$

Finding optimal $\mathbf{u}, \mathbf{v} \in \mathbb{R}^n$ reduces to the following unconstrained dual problem:

$$\underset{\mathbf{u}, \mathbf{v} \in \mathbb{R}^n}{\text{minimize}} \quad \sum_{ij} P(\mathbf{u}, \mathbf{v})_{ij} - \langle \mathbf{u}, \mathbf{r} \rangle - \langle \mathbf{v}, \mathbf{c} \rangle. \quad (4)$$

The SA algorithm (Alg. 3 in Appx. A) can be used to solve (4) and approximately project $\exp\{-\gamma C_{ij}\}$ onto $\mathcal{U}(\mathbf{r}, \mathbf{c})$ given a stopping criterion measured by a distance or divergence d . Sinkhorn updates are guaranteed to converge to dual-optimal values as the number of iterations $k \rightarrow \infty$ (Sinkhorn & Knopp, 1967; Sinkhorn, 1967; Franklin & Lorenz, 1989; Knight, 2008). Later, SA was shown to converge with complexity $\tilde{O}(n^2)$ with other terms depending on the level of desired accuracy (Altschuler et al., 2017). While the solution $P(\gamma)$ of (2) converges to the solution P^* of (1) as $\gamma \rightarrow \infty$, $\langle P(\gamma) - P^*, C \rangle$ is effectively bounded below in practice since entries $\exp\{-\gamma C_{ij}\}$ hit the machine precision limit, which causes numerical instabilities as γ grows (Cuturi, 2013).

2.3 Mirror Descent

To solve problem (1) reliably, we instead adopt mirror descent (Nemirovski & Yudin, 1983):

$$\mathbf{x}^{t+1} = \arg \min_{\mathbf{x} \in \mathcal{F} \cap \mathcal{D}} \{ \langle \nabla f(\mathbf{x}^t), \mathbf{x} \rangle + \frac{1}{\gamma_t} D_h(\mathbf{x} | \mathbf{x}^t) \}, \quad (5)$$

where \mathcal{F} is a feasible set ($\mathcal{U}(\mathbf{r}, \mathbf{c})$ in our case) and D_h is the Bregman divergence defined as follows:

$$D_h(\mathbf{y} | \mathbf{x}) = h(\mathbf{y}) - h(\mathbf{x}) - \langle \nabla h(\mathbf{x}), \mathbf{y} - \mathbf{x} \rangle, \quad (6)$$

given a strictly convex and differentiable function $h : \mathcal{D} \rightarrow \mathbb{R}$ called the *mirror map*. Equivalently:

$$\hat{\mathbf{x}}^{t+1} = \nabla h^{-1}(\nabla h(\mathbf{x}^t) - \gamma_t \nabla f(\mathbf{x}^t)) \quad (7)$$

$$\mathbf{x}^{t+1} = \arg \min_{\mathbf{x} \in \mathcal{F} \cap \mathcal{D}} D_h(\mathbf{x} | \hat{\mathbf{x}}^{t+1}). \quad (8)$$

Here, (7) takes a gradient step in the dual space and maps the new point back onto the primal space, while (8) defines a Bregman projection of $\hat{\mathbf{x}}^{t+1}$ onto the feasible set \mathcal{F} in the primal space. Throughout, we use $h(\mathbf{x}) = \sum_{i=1}^n x_i \log(x_i)$ in domain $\mathcal{D} = \mathbb{R}_{>0}^n$, which yields $D_h(\mathbf{y} | \mathbf{x}) = D_{\text{KL}}(\mathbf{y} | \mathbf{x})$ on the simplex Δ_n . In general, for $\mathbf{x}, \mathbf{y} \in \mathcal{D}$ we have $D_h(\mathbf{y} | \mathbf{x}) = \sum_i x_i - y_i + y_i \log(y_i/x_i)$.

2.4 Conjugate Gradients

While SA (Alg. 3) can be used to solve the Bregman projection problem given in (8) for the OT problem, we find that as MD step t grows, the convergence rate of SA declines. For an alternative solution, we turn to the non-linear conjugate gradients (NCG) method from the numerical optimization literature (Fletcher & Reeves, 1964; Nocedal & Wright, 2006). NCG methods take descent directions $\mathbf{p}^0 = -\nabla f(\mathbf{x}^0)$ and $\mathbf{p}^{k+1} \leftarrow -\nabla f(\mathbf{x}^k) + \beta_k \mathbf{p}^k$, and iterate $\mathbf{x}^{k+1} \leftarrow \mathbf{x}^k + \alpha \mathbf{p}^k$. Various formulas for computing β_k exist, which (given optimal α) guarantee convergence in at most n' iterations for quadratic objectives, where $n' \leq n$ is the number of distinct eigenvalues of $\nabla^2 f$. Further, the objective decreases faster if eigenvalues form a small number of tight clusters (Stiefel, 1958; Kaniel, 1966; Nocedal & Wright, 2006). The Polak-Ribiere (PR) method is especially relevant to our efforts:

$$\beta_k^{PR} = \frac{\langle \nabla f(\mathbf{x}^k) - \nabla f(\mathbf{x}^{k-1}), \nabla f(\mathbf{x}^k) \rangle}{\| \nabla f(\mathbf{x}^{k-1}) \|^2}. \quad (9)$$

The optimal α has a closed-form for quadratics, but for general non-linear objectives line search is necessary. We refer the reader to Appx. A.4 for relevant background on line search methods.

One practical way to improve the convergence rate of CG methods is via *preconditioning*. By making a change of variables $\mathbf{x} = S\hat{\mathbf{x}}$, one reduces the condition number of the problem and/or renders the eigenvalues of the reparametrized problem more tightly clustered for improved convergence (ideally, $SS^\top \approx (\nabla^2 f)^{-1}$). We refer the reader to Hager & Zhang (2006b) for further details on CG methods.

3 Solving Optimal Transport with Mirror Descent and Conjugate Gradients

3.1 Mirror Descent for Optimal Transport

Consider now the optimal transport problem with the objective function $f(P) = \langle P, C \rangle$ with a constant gradient $\nabla f(P) = C$. Given a convex function h , MD updates are given by:

$$P^{t+1} = \arg \min_{P \in \mathcal{U}(\mathbf{r}, \mathbf{c})} \left\{ \langle P, C \rangle + \frac{1}{\gamma_t} D_h(P|P^t) \right\}. \quad (10)$$

The following lemma predicts improvement given by (10) with equality (all proofs are in Appx. B).

Lemma 3.1. *Given $h(P) = \sum_{ij} P_{ij} \log P_{ij}$ and $P^t, P^{t+1} \in \mathcal{U}(\mathbf{r}, \mathbf{c})$ related via (10), we have*

$$\langle P^t, C \rangle - \langle P^{t+1}, C \rangle = \frac{1}{\gamma_t} (D_{\text{KL}}(P^t|P^{t+1}) + D_{\text{KL}}(P^{t+1}|P^t)). \quad (11)$$

Next, we provide an error guarantee for transport plans computed via (exact) mirror descent.

Proposition 3.2 (Mirror descent error bounds for optimal transport). *Let $[\gamma_t]_{t=0}^{T-1}$ be a sequence of step sizes with $\sum_{t=0}^{T-1} \gamma_t = \bar{\gamma}$. Given a plan P^0 followed by a sequence of T plans computed via (10):*

$$\langle P^T, C \rangle - \langle P^*, C \rangle \leq \frac{D_h(P^*|P^0)}{\bar{\gamma}}. \quad (12)$$

Furthermore, let $H_{\min} = \min(H(\mathbf{r}), H(\mathbf{c}))$. If $h(\mathbf{x}) = \sum_i x_i \log x_i$ and $P^0 = \mathbf{r}\mathbf{c}^\top$:

$$\langle P^T, C \rangle - \langle P^*, C \rangle \leq \frac{H_{\min}}{\bar{\gamma}}. \quad (13)$$

The bounds show that choosing $P^0 = \mathbf{r}\mathbf{c}^\top$ yields a tighter information-theoretic upper bound given by H_{\min} rather than a naive upper bound given by $\log_2 n$, which was used to select γ in prior work (Altschuler et al., 2017; Lin et al., 2022). Indeed, observe that if either of \mathbf{r} or \mathbf{c} is a delta distribution so that $H_{\min} = 0$, the bound in (13) is tight for any $\gamma > 0$ since the only feasible transport plan is the independence coupling in this case as all probability mass has to be transported from (to) a single source (sink). Hence, given $P^0 = \mathbf{r}\mathbf{c}^\top$ and $H_{\min} > 0$, we recommend that the sequence $[\gamma_t]_{t \in [1 \dots T]}$ be selected so that $\bar{\gamma}$ is proportional to H_{\min} . Secondly, the bounds highlight the need to use large $\bar{\gamma}$ to achieve low error for high-entropy distributions \mathbf{r}, \mathbf{c} (see also Appx. C of Kemertas & Jepson (2022), which shows a high correlation between H_{\min} and the relative error between inexact solutions of (1) and (2) for a fixed γ). Given the well-known numerical stability issues of SA for high γ , we seek to use MD with $T > 1$. We now present a lemma on the equivalence of transport plans computed via MD and entropic regularization.

Algorithm 1 MDOT($P^0, C, \mathbf{r}, \mathbf{c}, \epsilon, \gamma, T, d$)

```

1: Initialize  $t \leftarrow 0$ 
2:  $\mathbf{u} \leftarrow \mathbf{0}, \mathbf{v} \leftarrow \mathbf{0}$ 
3: while  $t < T$  do
4:    $t \leftarrow t + 1$ 
5:    $\hat{P}^t \leftarrow P^{t-1} \odot \exp\{-\gamma C\}$ 
6:    $P^t, \mathbf{u}, \mathbf{v} \leftarrow \text{BregProj}(\hat{P}^t, \mathbf{r}, \mathbf{c}, \epsilon, \mathbf{u}, \mathbf{v}, d)$ 
7: end while
8: Output  $P \leftarrow P^t$ 

```

Given $P^0 = \mathbf{r}\mathbf{c}^\top$ and $H_{\min} > 0$, we recommend that the sequence $[\gamma_t]_{t \in [1 \dots T]}$ be selected so that $\bar{\gamma}$ is proportional to H_{\min} . Secondly, the bounds highlight the need to use large $\bar{\gamma}$ to achieve low error for high-entropy distributions \mathbf{r}, \mathbf{c} (see also Appx. C of Kemertas & Jepson (2022), which shows a high correlation between H_{\min} and the relative error between inexact solutions of (1) and (2) for a fixed γ). Given the well-known numerical stability issues of SA for high γ , we seek to use MD with $T > 1$. We now present a lemma on the equivalence of transport plans computed via MD and entropic regularization.

Lemma 3.3. *Let $P_1, P_2 \in \mathcal{U}(\mathbf{r}, \mathbf{c})$ be computed over T_1 and T_2 steps of MD with arbitrary schedules γ_t such that the sum of MD step sizes equal $\bar{\gamma}$ for both given any initial plan $P^0 \in \mathbb{R}_{>0}^{n \times n}$ of rank 1. Further, let P_3 be the solution of problem (2) with $\gamma = \bar{\gamma}$. We have $P_1 = P_2 = P_3$.*

The question of how to compute (10) remains. Writing the Lagrangian dual for problem (10) and setting its partial derivative with respect to P_{ij} to 0 yields (cf. (3)):

$$P_{ij}(\mathbf{u}, \mathbf{v}) = P_{ij}^t \exp\{u_i + v_j - \gamma C_{ij}\}, \quad (14)$$

where $\mathbf{u}, \mathbf{v} \in \mathbb{R}^n$ and $P^t \in \mathbb{R}_{>0}^{n \times n}$. This yields the following dual objective:

$$g(\mathbf{u}, \mathbf{v}; P^t) = \sum_{ij} P_{ij}^t (\mathbf{u}_i + \mathbf{v}_j) - \langle \mathbf{u}, \mathbf{r} \rangle - \langle \mathbf{v}, \mathbf{c} \rangle - 1, \quad (15)$$

where any minimizer $(\mathbf{u}^*, \mathbf{v}^*)$ of g satisfies $P_{ij}^{t+1} = P_{ij}^t \exp\{u_i^* + v_j^* - \gamma C_{ij}\}$. That is, minimizing this objective corresponds precisely to the Bregman projection problem (8) with $\hat{P}^{t+1} = P^t \odot \exp\{-\gamma C\}$ being projected onto $\mathcal{U}(\mathbf{r}, \mathbf{c})$. This observation gives rise to the generalizing Mirror Descent Optimal Transport (MDOT) algorithm shown in Alg. 1. Here, one choice of a Bregman projection call (L6 of the algorithm) is Sinkhorn projection given by Alg. 3. In the next section, we introduce a new Bregman projection algorithm. A notable feature of Alg. 1 is that it initializes the optimization of g via the near-optimal dual variables from the previous iteration (warm-starting). This is motivated by the following corollary of Lemma 3.1.

Corollary 3.4. *Given the same setting as Lemma 3.1,*

$$\|P^{t+1} - P^t\|_1 \leq \min\left(\gamma_t, \sqrt{\frac{H_{\min} \gamma_t}{\sum_t \gamma_t}}\right). \quad (16)$$

Given fixed $\gamma_t = \gamma$, we have $\|P^{t+1} - P^t\|_1 \leq \min(\gamma, \sqrt{H_{\min}/t})$. Since the distance between consecutive transport plans shrinks with growing t , we expect the dual variables from the previous step to constitute an increasingly good initialization for the dual optimization in the next step (cf. (15)) under a fixed-rate schedule. This is empirically confirmed in Fig. 2 and discussed in Sec. 4. The Sinkhorn iteration approach discussed by Cuturi (2013) is a special case of Alg. 1 with $P^0 = \mathbf{1}_{n \times n}$ and $T = 1$. Differently, we will (i) make an intuitive choice of a strictly feasible initialization $P^0 = \mathbf{r}\mathbf{c}^\top$ to leverage information-theoretic guarantees of (13), and (ii) break down the problem into multiple steps with $T \geq 1$ to ensure high accuracy without compromising numerical stability.

As implied by (13), the latter is a particularly useful configuration when both \mathbf{r} and \mathbf{c} have high entropy. In that sense, while being equally simple to understand and implement, MDOT offers more flexibility by enabling entropy-aware choice of algorithm parameters (γ, T) , as well as a better trade-off between accuracy and numerical stability especially in the high-entropy/high-accuracy regime. Furthermore, we show in Sec. 4 that in some cases, $T > 1$ converges in fewer total Bregman projection steps than $T = 1$ for the same $\bar{\gamma}$ (cf. Lemma 3.3).

Algorithm 2 PNCGProject($P, \mathbf{r}, \mathbf{c}, \epsilon, \mathbf{u}, \mathbf{v}$)

```

1: Initialize  $k \leftarrow 0$ 
2:  $P^0 \leftarrow \mathbf{D}(\exp\{\mathbf{u}\})P\mathbf{D}(\exp\{\mathbf{v}\})$ 
3:  $\rho \leftarrow D_h(\mathbf{r}(P^0)|\mathbf{r}) + D_h(\mathbf{c}(P^0)|\mathbf{c})$ 
4: while  $\rho > \epsilon$  do
5:    $k \leftarrow k + 1$ 
6:   Evaluate  $\mathbf{s}^k$  ▷ (19)
7:    $\mathbf{p}^k \leftarrow -\mathbf{s}^k + \beta_k \mathbf{p}^{k-1}$  ▷ (21)
8:   if  $\langle \mathbf{p}^k, \nabla g^k \rangle < 0$  then
9:      $\mathbf{p}^k \leftarrow -\mathbf{s}^k$  ▷ Reset CG
10:   end if
11:    $\alpha_k \leftarrow \text{LSearch}(\mathbf{p}^k, P^k, \mathbf{u}, \mathbf{v}, \mathbf{r}, \mathbf{c}, \rho)$ 
12:    $\mathbf{u} \leftarrow \mathbf{u} + \alpha_k \mathbf{p}_u^k, \mathbf{v} \leftarrow \mathbf{v} + \alpha_k \mathbf{p}_v^k$ 
13:    $P^k \leftarrow \mathbf{D}(\exp\{\mathbf{u}\})P^0\mathbf{D}(\exp\{\mathbf{v}\})$ 
14:    $\rho \leftarrow D_h(\mathbf{r}(P^k)|\mathbf{r}) + D_h(\mathbf{c}(P^k)|\mathbf{c})$ 
15: end while
16: Output  $P^k, \mathbf{u}, \mathbf{v}$ 

```

3.2 Preconditioned Non-linear Conjugate Gradients for Approximate Bregman Projections

As mentioned earlier, the convergence rate of Sinkhorn iteration for solving problems (8) in MD declines with growing t . In Appx. B, we provide a proposition that applies Thm. 4 of Franklin & Lorenz (1989) on matrix scaling to our MD setting, which characterizes this behavior and motivates a new algorithm for minimizing (15) via conjugate gradients. To further study the dual objective g we consider its Hessian, which has the following block form:

$$\nabla^2 g(\mathbf{u}, \mathbf{v}) = \begin{pmatrix} \mathbf{D}(\mathbf{r}(P(\mathbf{u}, \mathbf{v}))) & P(\mathbf{u}, \mathbf{v}) \\ P(\mathbf{u}, \mathbf{v})^\top & \mathbf{D}(\mathbf{c}(P(\mathbf{u}, \mathbf{v}))) \end{pmatrix}. \quad (17)$$

The Hessian above and that of the objective in (4) are both degenerate with rank at most $2n - 1$. Indeed, there is an eigenvector $(\mathbf{1}_n, -\mathbf{1}_n)^\top$ with a zero eigenvalue. This degeneracy is due to the

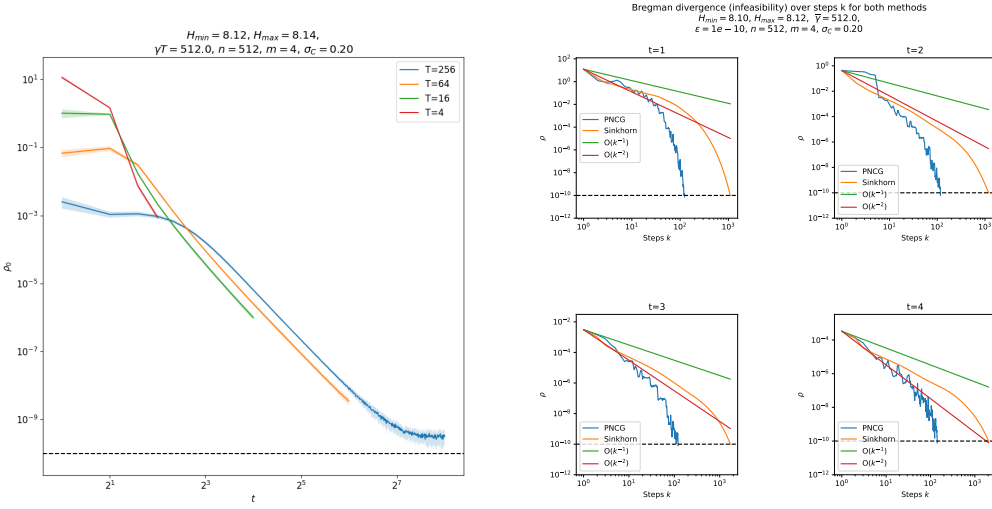


Figure 2: **(Left)** Decreasing initial infeasibility error ρ_0 over t MD steps under warm-starting dual variables (\mathbf{u}, \mathbf{v}) for varying T given fixed MD step size $\gamma_t = 512/T$. Shaded areas show 1 standard deviation across 32 samples of $(\mathbf{r}, \mathbf{c}, \mathbf{C})$. **(Right)** Infeasibility error of Bregman projection algorithms over dual variable update steps k for varying MD time-steps t . Sinkhorn iteration (orange) slows down as t grows, while the PNCG approach (blue) is more robust and consistently faster (converges $\approx 10 \times$ faster). Rates of $O(k^{-1})$ and $O(k^{-2})$ are displayed as baselines for visual comparison. Horizontal dashed line marks ϵ used as the stopping criterion.

well-known property that scalar shifts $\mathbf{u} + \delta \mathbf{1}_n$ and $\mathbf{v} - \delta \mathbf{1}_n$ yield the same $P(\mathbf{u}, \mathbf{v})$ and $g(\mathbf{u}, \mathbf{v})$ for any $\delta \in \mathbb{R}$, i.e., the objective is constant along this direction. Hence, when studying the scaling of the Hessian empirically, instead of the condition number λ_{2n}/λ_1 , we heuristically consider a *pseudo*-condition number λ_{2n}/λ_2 given eigenvalues $0 = \lambda_1 \leq \dots \leq \lambda_{2n}$.

While a straightforward application of NCG to the minimization of the objective given in (15) requires only computing the gradient with respect to \mathbf{u}, \mathbf{v} (omitting the dependence of g on P^t for brevity):

$$\nabla g(\mathbf{u}, \mathbf{v}) = (\mathbf{r}(P(\mathbf{u}, \mathbf{v})) - \mathbf{r}, \mathbf{c}(P(\mathbf{u}, \mathbf{v})) - \mathbf{c})^\top, \quad (18)$$

we instead consider replacing the gradient with the *Sinkhorn direction* to scale the Hessian:

$$s(\mathbf{u}, \mathbf{v}) = (\log \mathbf{r}(P(\mathbf{u}, \mathbf{v})) - \log \mathbf{r}, \log \mathbf{c}(P(\mathbf{u}, \mathbf{v})) - \log \mathbf{c})^\top. \quad (19)$$

It is easy to show that the (negative) Sinkhorn direction is always a descent direction:

$$\begin{aligned} \langle s(\mathbf{u}, \mathbf{v}), \nabla g(\mathbf{u}, \mathbf{v}) \rangle &= D_h(\mathbf{r}(P(\mathbf{u}, \mathbf{v}))|\mathbf{r}) + D_h(\mathbf{r}|\mathbf{r}(P(\mathbf{u}, \mathbf{v}))) \\ &\quad + D_h(\mathbf{c}(P(\mathbf{u}, \mathbf{v}))|\mathbf{c}) + D_h(\mathbf{c}|\mathbf{c}(P(\mathbf{u}, \mathbf{v}))) \geq 0. \end{aligned} \quad (20)$$

One interpretation of this choice of descent direction is as a preconditioning of the system. In particular, observe that $s(\mathbf{u}, \mathbf{v}) = M \nabla g(\mathbf{u}, \mathbf{v})$, where the diagonal preconditioner $M = \mathbf{D}(s(\mathbf{u}, \mathbf{v})/\nabla g(\mathbf{u}, \mathbf{v}))$. In Sec. 4, we empirically show that the pseudo-condition number of $M \nabla^2 g$ is markedly lower than that of $\nabla^2 g$ across a variety of problems and the preconditioned NCG (PNCG) approach behaves much better particularly over lower entropy marginals.

Given Sinkhorn directions s^k and gradients ∇g^k at each step k , we compute β_k via the following formula (cf. (9)) based on Al-Baali & Fletcher (1996) for *preconditioned* Polak-Ribiere (PPR):

$$\beta_k^{PPR} = \frac{\langle \nabla g^k - \nabla g^{k-1}, s^k \rangle}{\langle \nabla g^{k-1}, \mathbf{p}^{k-1} \rangle}, \quad (21)$$

where $\beta_1^{PPR} = 0$ (see Alg. 2). Details of the line search in L11 of Alg. 2 are deferred to Appx. C.

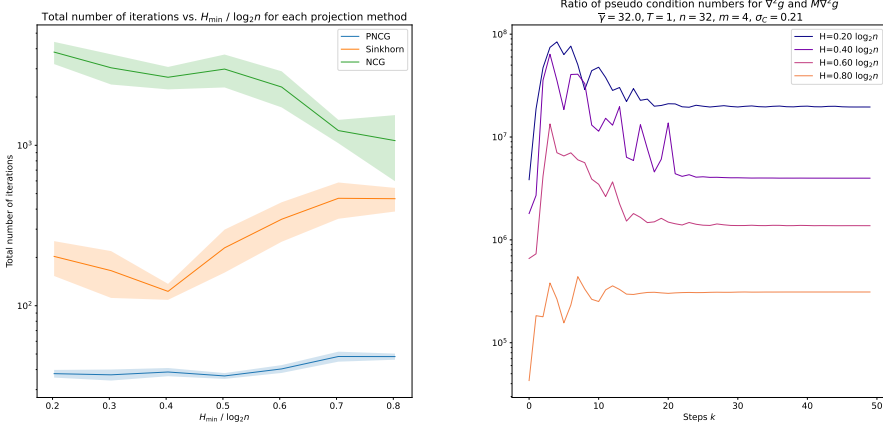


Figure 3: **(Left)** Avg. number of iterations over 32 runs for Sinkhorn (orange), PNCG (blue) and the vanilla NCG (green) algorithms vs. entropy level of marginals given $n = 8$, $m = 4$, $T = 1$, $\bar{\gamma} = 128$, $\epsilon = 10^{-5}$ and $H_{\min} \approx H(\mathbf{r}) \approx H(\mathbf{c})$. **(Right)** The ratio of pseudo condition numbers for the Hessian and the preconditioned Hessian over 50 iterations of PNCG given $n = 32$, $m = 4$, $T = 1$, $\bar{\gamma} = 32$ and $H_{\min} \approx H(\mathbf{r}) \approx H(\mathbf{c})$ averaged over 32 runs. Preconditioning is increasingly more effective in reducing the pseudo-condition number for lower entropy distributions. This behavior is strongly correlated with the number of iterations until convergence for NCG vs. PNCG shown on the left.

4 Experiments

In this section we first empirically investigate the questions listed below (Q1-5) on a synthetic dataset and present a comparative study of the behavior of proposed algorithms under various conditions involving desired level of accuracy and the entropy of target marginals:

1. Does warm-starting reduce the initial error of Bregman projections when $T > 1$?
2. Does Sinkhorn iteration maintain its high convergence rate for $t > 1$? How does it compare against the preconditioned NCG method?
3. Does employing Sinkhorn directions (preconditioning) instead of the vanilla NCG improve convergence speed of NCG? If so, under what conditions with respect to the entropy of \mathbf{r}, \mathbf{c} ?
4. Does MDOT (Alg. 1) converge in fewer projection steps for $T > 1$ than $T = 1$?
5. How does Sinkhorn iteration compare to the PNCG approach with varying ϵ ?¹

Then, in Sec. 4.2 we compare the algorithms discussed in this paper to SA and a recent algorithm by Ballu & Berthet (2022) over the MNIST dataset, which has been used as a benchmark in OT studies. All experiments are performed on an NVIDIA GeForce GTX 1080 GPU with 64-bit precision. All transport plans are *rounded* onto $\mathcal{U}(\mathbf{r}, \mathbf{c})$ via Alg. 2 of Altschuler et al. (2017) after processing.

4.1 Ablations and In Depth Analysis over Synthetic Datasets

For the empirical evaluations here, we sample a cost matrix C as follows. First, we uniformly sample $2n$ points on the unit ball in \mathbb{R}^m . Then we compute pairwise distances to construct a Euclidean distance matrix.² To constrain cost values to $[0, 1]$, we subtract the minimum distance value from each entry before normalizing the matrix by dividing all entries by the maximum value. To sample distributions \mathbf{r} and \mathbf{c} , we first determine target entropy values $H(\mathbf{r}) \approx H(\mathbf{c}) \in [0.1 \log n, 0.9 \log n]$ of interest. Then, we repeatedly sample a large number of distributions from the $(n - 1)$ -simplex via the Dirichlet distribution. The concentration parameters of the Dirichlet distribution are all equal; this constant is selected (with simple heuristics) to increase the likelihood that a distribution satisfying the entropy requirement is included among the samples. The procedure successfully terminates when distributions \mathbf{r} and \mathbf{c} with entropy values within a range of 0.01 of the target are found. Lastly, if the

¹We also vary n for a fixed ϵ in Appx. E and show similar dependence on n for Sinkhorn and PNCG.

²At this stage, pairwise distances are approximately distributed as a Gaussian $\mathcal{N}(\sqrt{2}, \frac{1}{2m})$ (Wu et al., 2017).

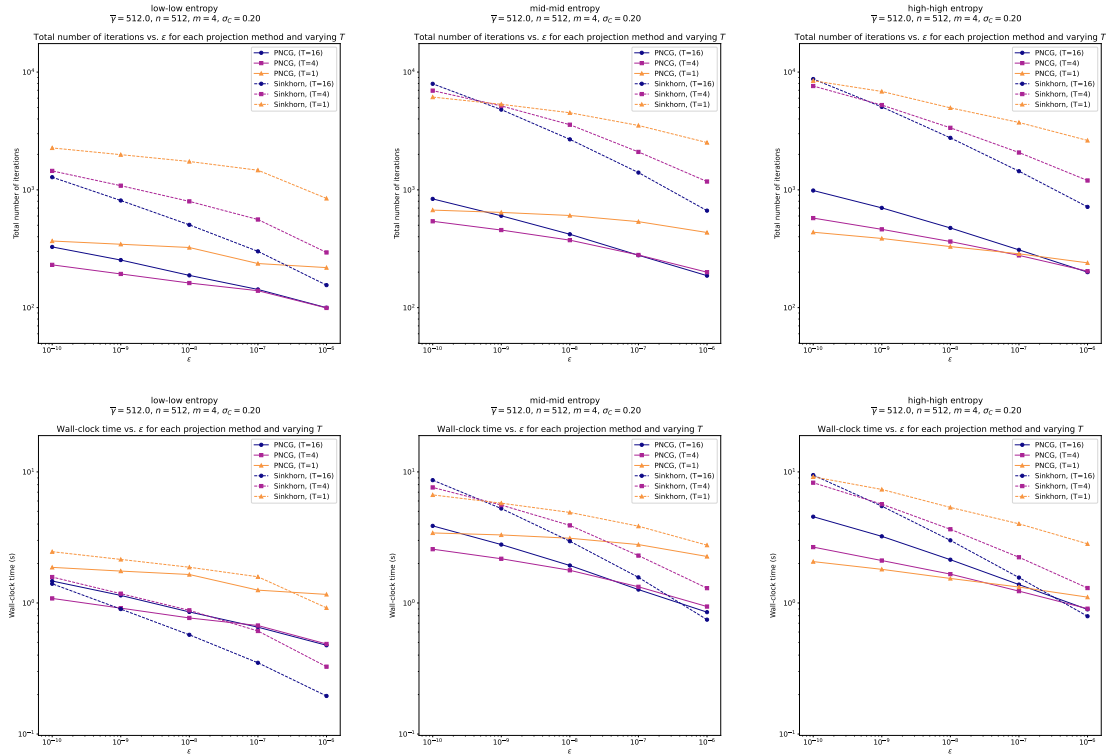


Figure 4: Number of iterations (**top**) and wall-clock time (**bottom**) vs. ϵ for Sinkhorn and PNCG projections given $n = 512$ and $T \in \{1, 4, 16\}$ over $H(\mathbf{r})$ and $H(\mathbf{c})$ both approximately $\{0.1 \log_2 n, 0.5 \log_2 n, 0.9 \log_2 n\}$ (**left-to-right**). PNCG consistently converges in fewer iterations. This yields significant gains in wall-clock time particularly in the high precision (small ϵ), high entropy setting. $T = 1$ is often sub-optimal and performs the worst particularly for Sinkhorn projections. Each marker is the average of 32 runs over sampled $(\mathbf{r}, \mathbf{c}, C)$. All plots are log-log scale.

distributions have entries smaller than 10^{-8} , we add 10^{-8} to each entry and re-normalize. Motivated by (13), this setup allows us to study the behavior of the algorithms discussed in this paper with respect to the marginal entropies in a controlled manner and show that this significantly impacts the number of iterations until convergence of the algorithms.

Q1-2. In Fig. 2, we first run the MDOT algorithm with PNCG for Bregman projections to show the effect of warm-starting (Q1 above) with $n = 512, m = 4, \bar{\gamma} = 512, \epsilon = 10^{-10}$ and $\gamma_t = 512/T$ where $T \in \{4, 16, 64, 256\}$ in the high entropy setting. Given $m = 4$, the cost matrix has standard deviation $\sigma_C \approx 0.2$. We sample 32 triplets of $(\mathbf{r}, \mathbf{c}, C)$ and plot the average of $\rho_0 = D_h(\mathbf{r}(P)|\mathbf{r}) + D_h(\mathbf{c}(P)|\mathbf{c})$ given initial P at each MD step. We see a clear advantage of warm-starting with ρ_0 decreasing consistently at a high rate in all settings of T . Next, we analyze Q2 in the same setup with $T = 4$ and show that PNCG consistently outperforms Sinkhorn iteration converging in roughly $10 \times$ fewer steps. Further, while Sinkhorn iteration slows down significantly with increasing t (to see this, compare the orange line to the $O(k^{-2})$ rate displayed in red across $t \in [1, 2, 3, 4]$), PNCG is more robust and converges at an avg. rate faster than $O(k^{-2})$ for all t .

Q3. In Fig. 3, we investigate Q3 by benchmarking the vanilla NCG approach against PNCG (as well as Sinkhorn projections). We sample 32 pairs of distributions from each of $\{0.2 \log_2 n, 0.4 \log_2 n, 0.6 \log_2 n, 0.8 \log_2 n\}$ entropy levels and run the projection algorithms. The results show that NCG is extremely slow for low-entropy distributions. Upon inspecting the Hessian in (17), we notice that for low entropy distributions, many rows (and columns) of the Hessian may consist entirely of near-zero entries when the marginals (\mathbf{r}, \mathbf{c}) are low-entropy (and therefore contain many near-zero entries), thus making the *approximate* rank of the Hessian much smaller than n . Indeed, on the right hand side of the same figure, we plot the ratio of the pseudo-condition number for $\nabla^2 g$ and $M \nabla^2 g$ over PNCG iterations (averaged over 32 samples of $(\mathbf{r}, \mathbf{c}, C)$ at each entropy level), and show that the preconditioning vastly reduces λ_{2n}/λ_2 ; the extent of reduction gradually increases with lower entropy distributions. However, even in the high entropy setting where the

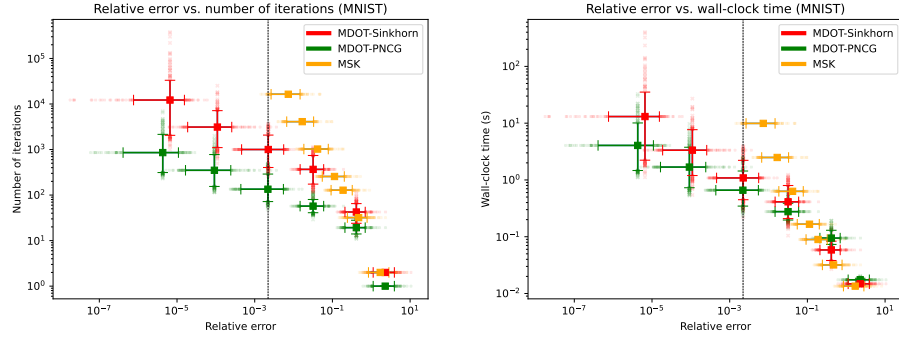


Figure 5: Total number of projection iterations (**left**) and wall-clock time (**right**) against relative error $\langle P - P^*, C \rangle / \langle P^*, C \rangle$ over the MNIST dataset. For MDOT, $\epsilon = \min(10^{-5}, 10^{-5} \times (H_{\min}/\bar{\gamma})^2)$ and $\bar{\gamma} \in \{2^0, 2^5, 2^7, 2^8, 2^9, 2^{12}\}$ with $\gamma_t = \bar{\gamma}/\max(1, \lfloor \bar{\gamma}/256 \rfloor)$ for all t in all experiments. For the Mirror Sinkhorn (MSK) alg. of [Ballu & Berthet \(2022\)](#), we fix the total number of iterations at each displayed marker on the left. Vertical and horizontal error bars mark 5th to 95th percentile confidence intervals among the 512 sample pairs (\mathbf{r}, \mathbf{c}) for respective axes, solid squares mark the mean values and outliers are shown as faded dots. Dashed vertical line marks the best relative error that can be achieved given $\bar{\gamma} = 256$ with $T = 1$; beyond this point numerical instabilities arise unless $T > 1$.

preconditioning has a milder effect, PNCG still outperforms NCG (as well as Sinkhorn projections) by a large margin. Thus the results suggest that preconditioning, which comes at no additional cost owing to a diagonal preconditioner, is essential for NCG algorithms to be broadly effective for OT. While the experiments here use relatively small $n, \bar{\gamma}$ and high ϵ due to the high computational cost of NCG in the low entropy setting and the cost of eigenvalue decomposition, we confirmed the same trends in high dimension - high precision cases over a few preliminary experiments not reported here.

Q4-5. In Fig. 4, we fix $\bar{\gamma} = 512$, $n = 512$, $m = 4$ and evaluate Sinkhorn and PNCG projections over low, mid and high entropy marginals while ablating $\epsilon \in \{10^{-6}, 10^{-7}, 10^{-8}, 10^{-9}, 10^{-10}\}$ over $T \in \{1, 4, 16\}$, where a fixed step size schedule $\gamma_t = \bar{\gamma}/T$ is used. Once again, each point on the plot marks the average over 32 samples of $(\mathbf{r}, \mathbf{c}, C)$. We find that for Sinkhorn projections, the performance of MDOT improves with increasing T both in terms of number of total projection iterations and wall-clock time (although $T > 16$ results in poorer performance not displayed in the figure). For PNCG, we do not observe such a clear pattern, but often $T = 1$ is still sub-optimal. PNCG converges in fewer iterations (up to 10 \times) with the performance gap widening as the marginal entropies increase. With the added cost of line search, while the wall-clock time of PNCG and Sinkhorn projections are comparable for low-entropy marginals ("easy" OT problems) and high ϵ (imprecise estimates of the distance), for harder OT problems and more precise estimates, the gains in terms of wall-clock time are substantial (up to 5 \times) particularly as the entropy levels of the marginals grow. We also observe better dependence of PNCG on ϵ , as the curves for the same T value have lower slope for PNCG (seen clearly upon visual inspection of both top and bottom rows).

4.2 Benchmarking on the MNIST Dataset

In this section, we evaluate the PNCG approach and the MDOT algorithm on the MNIST dataset in line with prior work ([Cuturi, 2013](#); [Altschuler et al., 2017](#); [Lin et al., 2022](#)). The cost matrix C is constructed by measuring the L_1 distance between 28×28 pixel locations on a 2D grid and dividing all entries by the maximum distance value so that $C_{ij} \in [0, 1]$. Images are converted to distributions by first flattening the 28×28 matrices of pixel intensity values, followed by injection of uniform noise $\mathcal{U}(0, 10^{-6})$ to form dense vectors and subsequent L_1 normalization. We randomly sample 1024 images without replacement, and compute a total of 512 OT distances between the first and second halves of the samples.³ When determining the step size schedule, we use the formula $\gamma_t = \bar{\gamma}/\max(1, \lfloor \bar{\gamma}/256 \rfloor)$, i.e., we take the largest power of 2 fixed step size possible until numerical errors are encountered, which occurs when $\gamma_t > 256$ in our setup (recommended for practitioners).

³We also measure the entropy of the sampled MNIST distributions and find that the entropy values are tightly clustered around $0.73 * \log_2(28^2)$, i.e., they largely fall in a mid-high range of entropy values.

In Fig. 5, we show that PNCG converges in $\approx 10\times$ fewer iterations than Sinkhorn in the high precision regime. While the added cost of line search slightly offsets the gains by a factor of 2 – 3 times, PNCG is still considerably faster in terms of wall-clock time except in the very high relative error range, where the errors are 25% or larger and therefore the estimates are of questionable utility. Notice also that the Sinkhorn projection algorithm is more susceptible to extremely slow convergence in some edge cases especially in the high precision regime as seen upon close inspection of outliers. We additionally compare to the closely related Mirror Sinkhorn (MSK) algorithm of [Ballu & Berthet \(2022\)](#) using the variable step size schedule prescribed by their Thm. 3.3; we find that their approach is competitive in the range where relative errors are above 10%, but performance degrades quickly with much poorer dependence on relative error for more precise computations.

5 Conclusion

In this work, we first presented a generalization of SA based on MD for computing high accuracy upper bounds on optimal transport distances. The algorithm employs a warm-starting of dual variables for Bregman projection problems in MD, which was empirically shown to be highly effective. While this generalization is agnostic to the particular choice of Bregman projection algorithm used, we showed that Sinkhorn iteration is not particularly well-suited to this setting and suffers from a declining convergence rate as MD proceeds in multiple steps. To address the issue, we presented a new conjugate gradients algorithm for Bregman projections. The algorithm was shown to outperform Sinkhorn iteration consistently by up to $10\times$ in terms of number of iterations until convergence for synthetic and real datasets, and desired accuracy levels. In terms of wall-clock time, the algorithm is especially well-suited for hard OT problems involving high-entropy marginals. While we focused on MD with a fixed learning rate, future work may consider variable learning rate MD procedures that exploit the warm-starting of the dual variables optimally. Similarly, we fixed the threshold for Bregman projection stopping criterion ϵ across all MD steps, while variable rate schedules may be more efficient. Faster and more precise line search procedures may further improve the performance of the new Bregman projection algorithm both in terms of number of iterations and wall-clock time.

Acknowledgements. Amir-massoud Farahmand acknowledges the funding from the Canada CIFAR AI Chairs program, as well as the support of the Natural Sciences and Engineering Research Council of Canada (NSERC) through the Discovery Grant program (2021-03701). Resources used in preparing this research were provided, in part, by the Province of Ontario, the Government of Canada through CIFAR, and companies sponsoring the Vector Institute. Mete Kemertas acknowledges the support of NSERC via the Canada Graduate Scholarship - Doctoral program (CGSD3-568998-2022). We would also like to thank the members of the Adaptive Agents Lab who provided feedback on a draft of this paper.

References

Mehiddin Al-Baali. Descent property and global convergence of the Fletcher—Reeves method with inexact line search. *IMA Journal of Numerical Analysis*, 5(1):121–124, 1985.

Mehiddin Al-Baali and Robert Fletcher. On the order of convergence of preconditioned nonlinear conjugate gradient methods. *SIAM Journal on Scientific Computing*, 17(3):658–665, 1996.

Jason Altschuler, Jonathan Niles-Weed, and Philippe Rigollet. Near-linear time approximation algorithms for optimal transport via sinkhorn iteration. In I. Guyon, U. Von Luxburg, S. Bengio, H. Wallach, R. Fergus, S. Vishwanathan, and R. Garnett (eds.), *Advances in Neural Information Processing Systems*, volume 30. Curran Associates, Inc., 2017. URL https://proceedings.neurips.cc/paper_files/paper/2017/file/491442df5f88c6aa018e86dac21d3606-Paper.pdf.

Neculai Andrei. *Nonlinear conjugate gradient methods for unconstrained optimization*. Springer, 2020.

Marin Ballu and Quentin Berthet. Mirror Sinkhorn: Fast online optimization on transport polytopes. *arXiv preprint arXiv:2211.10420*, 2022.

Sébastien Bubeck. Convex optimization: Algorithms and complexity. *Foundations and Trends® in Machine Learning*, 8(3-4):231–357, 2015.

Thomas M. Cover and Joy A. Thomas. *Elements of Information Theory (Wiley Series in Telecommunications and Signal Processing)*. Wiley-Interscience, USA, 2006. ISBN 0471241954.

Marco Cuturi. Sinkhorn distances: Lightspeed computation of optimal transport. In C.J. Burges, L. Bottou, M. Welling, Z. Ghahramani, and K.Q. Weinberger (eds.), *Advances in Neural Information Processing Systems*, volume 26. Curran Associates, Inc., 2013. URL https://proceedings.neurips.cc/paper_files/paper/2013/file/af21d0c97db2e27e13572cbf59eb343d-Paper.pdf.

Robert Dadashi, Leonard Hussenot, Matthieu Geist, and Olivier Pietquin. Primal Wasserstein imitation learning. In *International Conference on Learning Representations*, 2021. URL <https://openreview.net/forum?id=TtYSU29zgR>.

Pavel Dvurechensky, Alexander Gasnikov, and Alexey Kroshnin. Computational optimal transport: Complexity by accelerated gradient descent is better than by Sinkhorn’s algorithm. In Jennifer Dy and Andreas Krause (eds.), *Proceedings of the 35th International Conference on Machine Learning*, volume 80 of *Proceedings of Machine Learning Research*, pp. 1367–1376. PMLR, 10–15 Jul 2018. URL <https://proceedings.mlr.press/v80/dvurechensky18a.html>.

Norm Ferns, Prakash Panangaden, and Doina Precup. Metrics for finite Markov decision processes. In *Proceedings of the 20th Conference on Uncertainty in Artificial Intelligence*, UAI ’04, pp. 162–169, Arlington, Virginia, USA, 2004. AUAI Press. ISBN 0974903906.

Rémi Flamary, Nicolas Courty, Alexandre Gramfort, Mokhtar Z Alaya, Aurélie Boisbunon, Stanislas Chambon, Laetitia Chapel, Adrien Corenflos, Kilian Fatras, Nemo Fournier, et al. POT: Python optimal transport. *The Journal of Machine Learning Research*, 22(1):3571–3578, 2021.

Reeves Fletcher and Colin M Reeves. Function minimization by conjugate gradients. *The computer journal*, 7(2):149–154, 1964.

George E Forsythe, Magnus R Hestenes, and J Barkley Rosser. Iterative methods for solving linear equations. In *Bulletin of the American Mathematical Society*, volume 57, pp. 480–480. AMER MATHEMATICAL SOC 201 CHARLES ST, PROVIDENCE, RI 02940-2213, 1951.

Leslie Fox, Harry D Huskey, and James Hardy Wilkinson. Notes on the solution of algebraic linear simultaneous equations. *The Quarterly Journal of Mechanics and Applied Mathematics*, 1(1):149–173, 1948.

Joel Franklin and Jens Lorenz. On the scaling of multidimensional matrices. *Linear Algebra and its applications*, 114:717–735, 1989.

Aude Genevay, Lénaïc Chizat, Francis Bach, Marco Cuturi, and Gabriel Peyré. Sample complexity of Sinkhorn divergences. In Kamalika Chaudhuri and Masashi Sugiyama (eds.), *Proceedings of the Twenty-Second International Conference on Artificial Intelligence and Statistics*, volume 89 of *Proceedings of Machine Learning Research*, pp. 1574–1583. PMLR, 16–18 Apr 2019. URL <https://proceedings.mlr.press/v89/genevay19a.html>.

Jean Charles Gilbert and Jorge Nocedal. Global convergence properties of conjugate gradient methods for optimization. *SIAM Journal on optimization*, 2(1):21–42, 1992.

Ishaan Gulrajani, Faruk Ahmed, Martin Arjovsky, Vincent Dumoulin, and Aaron C Courville. Improved training of wasserstein gans. In I. Guyon, U. Von Luxburg, S. Bengio, H. Wallach, R. Fergus, S. Vishwanathan, and R. Garnett (eds.), *Advances in Neural Information Processing Systems*, volume 30. Curran Associates, Inc., 2017. URL https://proceedings.neurips.cc/paper_files/paper/2017/file/892c3b1c6dccc52936e27cbd0ff683d6-Paper.pdf.

Sergey Guminov, Pavel Dvurechensky, Nazarii Tupitsa, and Alexander Gasnikov. On a combination of alternating minimization and Nesterov’s momentum. In Marina Meila and Tong Zhang (eds.), *Proceedings of the 38th International Conference on Machine Learning*, volume 139 of *Proceedings of Machine Learning Research*, pp. 3886–3898. PMLR, 18–24 Jul 2021. URL <https://proceedings.mlr.press/v139/guminov21a.html>.

William W Hager and Hongchao Zhang. CG DESCENT, a conjugate gradient method with guaranteed descent. *ACM Transactions on Mathematical Software (TOMS)*, 32(1):113–137, 2006a.

William W Hager and Hongchao Zhang. A survey of nonlinear conjugate gradient methods. *Pacific journal of Optimization*, 2(1):35–58, 2006b.

Magnus R Hestenes and Eduard Stiefel. Methods of conjugate gradients for solving linear systems. *Journal of research of the National Bureau of Standards*, 49(6):409–436, 1952.

Kirthevasan Kandasamy, Willie Neiswanger, Jeff Schneider, Barnabas Poczos, and Eric P Xing. Neural architecture search with bayesian optimisation and optimal transport. In S. Bengio, H. Wallach, H. Larochelle, K. Grauman, N. Cesa-Bianchi, and R. Garnett (eds.), *Advances in Neural Information Processing Systems*, volume 31. Curran Associates, Inc., 2018. URL https://proceedings.neurips.cc/paper_files/paper/2018/file/f33ba15effa5c10e873bf3842afb46a6-Paper.pdf.

Shmuel Kaniel. Estimates for some computational techniques in linear algebra. *Mathematics of Computation*, 20(95):369–378, 1966.

Mete Kemertas and Allan Douglas Jepson. Approximate policy iteration with bisimulation metrics. *Transactions on Machine Learning Research*, 2022. URL <https://openreview.net/forum?id=Ii7UeHc0m0>.

Philip A Knight. The Sinkhorn–Knopp algorithm: convergence and applications. *SIAM Journal on Matrix Analysis and Applications*, 30(1):261–275, 2008.

Nathaniel Lahn, Deepika Mulchandani, and Sharath Raghvendra. A graph theoretic additive approximation of optimal transport. In H. Wallach, H. Larochelle, A. Beygelzimer, F. d’Alché-Buc, E. Fox, and R. Garnett (eds.), *Advances in Neural Information Processing Systems*, volume 32. Curran Associates, Inc., 2019. URL https://proceedings.neurips.cc/paper_files/paper/2019/file/9b07f50145902e945a1cc629f729c213-Paper.pdf.

Yin Tat Lee and Aaron Sidford. Path finding methods for linear programming: Solving linear programs in $\tilde{O}(\sqrt{\text{rank}})$ iterations and faster algorithms for maximum flow. In *2014 IEEE 55th Annual Symposium on Foundations of Computer Science*, pp. 424–433, 2014.

Tianyi Lin, Nhat Ho, and Michael Jordan. On efficient optimal transport: An analysis of greedy and accelerated mirror descent algorithms. In Kamalika Chaudhuri and Ruslan Salakhutdinov (eds.), *Proceedings of the 36th International Conference on Machine Learning*, volume 97 of *Proceedings of Machine Learning Research*, pp. 3982–3991. PMLR, 09–15 Jun 2019. URL <https://proceedings.mlr.press/v97/lin19a.html>.

Tianyi Lin, Nhat Ho, and Michael I. Jordan. On the efficiency of entropic regularized algorithms for optimal transport. *Journal of Machine Learning Research*, 23(137):1–42, 2022. URL <https://jmlr.org/papers/v23/20-277.html>.

Arkadi Nemirovski and Dmitry Yudin. Problem complexity and method efficiency in optimization. *John Wiley & Sons*, 1983.

Jorge Nocedal and Stephen J. Wright. *Numerical Optimization*. Springer, New York, NY, USA, 2e edition, 2006.

James B Orlin. A polynomial time primal network simplex algorithm for minimum cost flows. *Mathematical Programming*, 78:109–129, 1997.

Gabriel Peyré, Marco Cuturi, et al. Computational optimal transport: With applications to data science. *Foundations and Trends® in Machine Learning*, 11(5-6):355–607, 2019.

Richard Sinkhorn. Diagonal equivalence to matrices with prescribed row and column sums. *The American Mathematical Monthly*, 74(4):402–405, 1967.

Richard Sinkhorn and Paul Knopp. Concerning nonnegative matrices and doubly stochastic matrices. *Pacific Journal of Mathematics*, 21(2):343–348, 1967.

Eduard L Stiefel. Kernel polynomials in linear algebra and their numerical applications. *Nat. Bur. Standards Appl. Math. Ser.*, 49:1–22, 1958.

Jan van den Brand, Yin Tat Lee, Yang P. Liu, Thatchaphol Saranurak, Aaron Sidford, Zhao Song, and Di Wang. Minimum cost flows, MDPs, and L1-regression in nearly linear time for dense instances. In *Proceedings of the 53rd Annual ACM SIGACT Symposium on Theory of Computing*, STOC 2021, pp. 859–869. Association for Computing Machinery, 2021.

Philip Wolfe. Convergence conditions for ascent methods. *SIAM review*, 11(2):226–235, 1969.

Philip Wolfe. Convergence conditions for ascent methods. ii: Some corrections. *SIAM review*, 13(2):185–188, 1971.

Chao-Yuan Wu, R Manmatha, Alexander J Smola, and Philipp Krahenbuhl. Sampling matters in deep embedding learning. In *Proceedings of the IEEE international conference on computer vision*, pp. 2840–2848, 2017.

Yujia Xie, Xiangfeng Wang, Ruijia Wang, and Hongyuan Zha. A fast proximal point method for computing exact Wasserstein distance. In Ryan P. Adams and Vibhav Gogate (eds.), *Proceedings of The 35th Uncertainty in Artificial Intelligence Conference*, volume 115 of *Proceedings of Machine Learning Research*, pp. 433–453. PMLR, 22–25 Jul 2020. URL <https://proceedings.mlr.press/v115/xie20b.html>.

Lei Yang and Kim-Chuan Toh. Bregman proximal point algorithm revisited: A new inexact version and its inertial variant. *SIAM Journal on Optimization*, 32(3):1523–1554, 2022.

Guus Zoutendijk. Nonlinear programming: a numerical survey. *SIAM Journal on Control*, 4(1):194–210, 1966.

Guus Zoutendijk. Nonlinear programming, computational methods. *Integer and nonlinear programming*, pp. 37–86, 1970.

A Background (Extended Version)

A.1 Optimal Transport

Given a cost matrix $C \in [0, 1]^{n \times n}$, where C_{ij} is the cost of transportation between $\mathbf{x}_i, \mathbf{x}_j \in \mathcal{X}$, and marginal distributions $\mathbf{r}, \mathbf{c} \in \Delta_n$, we study the optimal transport problem given by the following:

$$\underset{P \in \mathcal{U}(\mathbf{r}, \mathbf{c})}{\text{minimize}} \quad \langle P, C \rangle. \quad (1 \text{ revisited})$$

Since the problem is a linear program (LP), the optimal transport plan need not be unique. Entropic regularization of the problem is often used for more efficient computation on GPUs (Cuturi, 2013):

$$\underset{P \in \mathcal{U}(\mathbf{r}, \mathbf{c})}{\text{minimize}} \quad \langle P, C \rangle - \frac{1}{\gamma} H(P) \quad (2 \text{ revisited})$$

where $\gamma > 0$ and $H(P) = -\sum_{ij} P_{ij} \log P_{ij}$ is the Shannon entropy of the joint distribution P , hence the term *entropic* regularization. The formulation is derived by adding an additional KL divergence constraint to (1) requiring $D_{\text{KL}}(P \mid \mathbf{r}\mathbf{c}^\top) \leq \zeta$, where $\mathbf{r}\mathbf{c}^\top$ is the independent coupling of (\mathbf{r}, \mathbf{c}) , $\zeta > 0$, and $D_{\text{KL}}(P \mid \mathbf{r}\mathbf{c}^\top) = \sum_{ij} P_{ij} \log \left(\frac{P_{ij}}{r_i c_j} \right)$ with the convention that $0/0 = 1$. The Lagrangian for the primal problem in (2) is given by the following,

$$\mathcal{L}(P, \boldsymbol{\alpha}, \boldsymbol{\beta}, \gamma) = \langle P, C \rangle + \langle \boldsymbol{\alpha}, \mathbf{r} - P\mathbf{1}_n \rangle + \langle \boldsymbol{\beta}, \mathbf{c} - P^T\mathbf{1}_n \rangle - \frac{1}{\gamma} H(P), \quad (22)$$

where $\boldsymbol{\alpha}, \boldsymbol{\beta} \in \mathbb{R}^n$ are dual variables and a smaller γ corresponds to a larger ζ . The negative entropy term renders the Lagrangian strictly convex in P , for which a unique solution with respect to P can be shown to exist with ease:

$$\frac{\partial \mathcal{L}}{\partial P_{ij}} = C_{ij} - \alpha_i - \beta_j + \frac{1}{\gamma} (1 + \log P_{ij}) = 0 \iff P_{ij} = e^{\gamma\alpha_i - 1/2} e^{-\gamma C_{ij}} e^{\gamma\beta_j - 1/2}. \quad (23)$$

With a reparametrization choosing $u_i = \gamma\alpha_i - 1/2$ and $v_j = \gamma\beta_j - 1/2$, plugging P_{ij} given by (3) into the Lagrangian results in the following unconstrained dual problem:

$$\underset{\mathbf{u}, \mathbf{v} \in \mathbb{R}^n}{\text{minimize}} \quad \sum_{ij} \exp \{u_i + v_j - \gamma C_{ij}\} - \langle \mathbf{u}, \mathbf{r} \rangle - \langle \mathbf{v}, \mathbf{c} \rangle \quad (24)$$

The SA algorithm (see Alg. 3) can be used to optimize this objective and approximately project $\exp \{-\gamma C_{ij}\}$ onto $\mathcal{U}(\mathbf{r}, \mathbf{c})$ given some stopping criterion measured by a distance or divergence d . The updates are guaranteed to converge to dual-optimal values as the number of iterations $k \rightarrow \infty$ (Sinkhorn & Knopp, 1967; Sinkhorn, 1967; Franklin & Lorenz, 1989; Knight, 2008). Later, the procedure and its variants were shown to converge in $\tilde{O}(n^2)$ iterations with other terms depending on the level of desired accuracy (Altschuler et al., 2017). While the optimal solution of (2) converges to the solution of (1) as $\gamma \rightarrow \infty$, there is a de-facto limit on the accuracy of the best possible upper bound that can be computed via 2 since entries $\exp \{-\gamma C_{ij}\}$ hit the machine precision limit quickly as γ grows (Cuturi, 2013).

A.2 Mirror Descent

To solve problem (1), we rely on mirror descent. Hence, we introduce the necessary background in this section. Originally proposed by Nemirovski & Yudin (1983), mirror descent can be viewed as

a generalization of gradient descent. To establish the connection, we first need to define Bregman divergences. Let $\mathcal{D} \subset \mathbb{R}^n$ be a convex, open set. The Bregman divergence between a pair of points $\mathbf{x}, \mathbf{y} \in \mathcal{D}$ under a strictly convex and differentiable function $h : \mathcal{D} \rightarrow \mathbb{R}$ is given by

$$D_h(\mathbf{y}|\mathbf{x}) = h(\mathbf{y}) - h(\mathbf{x}) - \langle \nabla h(\mathbf{x}), \mathbf{y} - \mathbf{x} \rangle. \quad (6 \text{ revisited})$$

That is, the Bregman divergence $D_h(\mathbf{y}|\mathbf{x})$ is the difference between $h(\mathbf{y})$ and its first-order approximation around \mathbf{x} . Since h is convex by construction, the divergence value is always non-negative (by the first-order condition for convexity). Then, given a non-empty convex set \mathcal{F} of feasible points such that \mathcal{F} is included in the closure of \mathcal{D} and $\mathcal{F} \cap \mathcal{D} \neq \emptyset$, an objective function $f : \mathbb{R}^n \rightarrow \mathbb{R}$ and an initial $\mathbf{x}^0 \in \mathcal{D}$, mirror descent algorithms perform the following updates:

$$\mathbf{x}^{t+1} = \arg \min_{\mathbf{x} \in \mathcal{F} \cap \mathcal{D}} \{ \langle \nabla f(\mathbf{x}^t), \mathbf{x} \rangle + \frac{1}{\gamma_t} D_h(\mathbf{x}|\mathbf{x}^t) \}, \quad (5 \text{ revisited})$$

where $\gamma_t^{-1} > 0$ is a (possibly time-varying) regularization weight. Equivalently:

$$\hat{\mathbf{x}}^{t+1} = \nabla h^{-1}(\nabla h(\mathbf{x}^t) - \gamma_t \nabla f(\mathbf{x}^t)) \quad (7 \text{ revisited})$$

$$\mathbf{x}^{t+1} = \arg \min_{\mathbf{x} \in \mathcal{F} \cap \mathcal{D}} D_h(\mathbf{x}|\hat{\mathbf{x}}^{t+1}), \quad (8 \text{ revisited})$$

where h is strictly convex and $\nabla h : \mathcal{D} \rightarrow \mathbb{R}^n$ is called the *mirror map* as it maps \mathbf{x} from the primal to the dual space. Here, (7) takes a gradient step in the dual space and maps the new point back onto the primal space, while (8) defines a Bregman projection of $\hat{\mathbf{x}}^{t+1}$ onto the feasible set \mathcal{F} in the primal space. For further technical definitions and requirements on h to ensure the existence and uniqueness of Bregman projections, see §4.1 of [Bubeck \(2015\)](#).

In the unconstrained case (i.e., $\mathcal{F} = \mathcal{D}$) with $h(\mathbf{x}) = \frac{1}{2} \|\mathbf{x}\|_2^2$ (which yields $D_h(\mathbf{y}|\mathbf{x}) = \frac{1}{2} \|\mathbf{y} - \mathbf{x}\|_2^2$ and $\nabla h(\mathbf{x}) = \mathbf{x}$), one recovers the standard gradient descent algorithm with step sizes γ_t . Otherwise, a Bregman projection onto \mathcal{F} as in (8) is necessary if the minimizer in \mathcal{D} lies outside \mathcal{F} , in which case one recovers the projected gradient descent method (once again) for $h(\mathbf{x}) = \frac{1}{2} \|\mathbf{x}\|_2^2$. Another common choice for h is the negative entropy $h(\mathbf{x}) = \sum_{i=1}^n x_i \log(x_i)$, which yields $D_h(\mathbf{y}|\mathbf{x}) = D_{\text{KL}}(\mathbf{y}|\mathbf{x})$ on the simplex Δ_n . In general, for $\mathbf{x}, \mathbf{y} \in \mathbb{R}_{>0}^n$ we have $D_h(\mathbf{y}|\mathbf{x}) = \sum_i x_i - y_i + y_i \log(y_i/x_i)$. Since the OT objective in (1) is linear, we state the following result of interest.

Lemma A.1 (A mirror descent bound for linear objectives). *Given a linear objective function $f(\mathbf{x}) = \langle \mathbf{x}, \mathbf{w} \rangle$, an initial point $\mathbf{x}^0 \in \mathcal{F}$, an optimal point \mathbf{x}^* and any $T > 0$, a sequence $[\mathbf{x}^t]_{t \in \mathbb{N}}$ obtained via (5) satisfies:*

$$f(\mathbf{x}^T) - f(\mathbf{x}^*) \leq \frac{D_h(\mathbf{x}^*|\mathbf{x}^0)}{\sum_{t=0}^{T-1} \gamma_t}. \quad (25)$$

For the proof, see Appx. B.

A.3 Conjugate Gradients

While Alg. 3 can be used to solve the Bregman projection problem given in (8) for the OT problem, we empirically and theoretically find that as mirror descent step t grows, the convergence rate of Sinkhorn iteration declines. To seek an alternative solution, we turn to the conjugate gradients approach from the numerical optimization literature, which we discuss in this section.

Initially proposed to solve linear systems of equations, or equivalently, unconstrained quadratic minimization problems, conjugate gradient (CG) methods aim to bridge steepest descent methods and Newton's method in terms of convergence properties while retaining low memory and computational requirements ([Fox et al., 1948](#); [Forsythe et al., 1951](#); [Hestenes & Stiefel, 1952](#)). Later, they were extended for minimization of general non-linear objectives by [Fletcher & Reeves \(1964\)](#). In the context of quadratic minimization, one ensures the conjugacy property between all descent directions $\mathbf{p}^k \in \mathbb{R}^n$ up to and including the k^{th} step, namely by requiring that they satisfy $(\mathbf{p}^k)^\top H \mathbf{p}^{k'} = 0$ for any $k, k' \in [1 \dots k]$ and $k \neq k'$, where $H \in \mathbb{R}^{n \times n}$ is the Hessian of the quadratic $f : \mathbb{R}^n \rightarrow \mathbb{R}$. It is well-known that when such descent directions are generated, the iterates $\mathbf{x}^{k+1} \leftarrow \mathbf{x}^k + \alpha \mathbf{p}^k$ with the step size $\alpha \in \mathbb{R}$ chosen to be the minimizer of the 1D quadratic along \mathbf{p}^k will converge to the

optimum in at most n steps (Nocedal & Wright, 2006). Furthermore, if the number m of distinct eigenvalues of H is less than n , the method converges in m iterations instead, while in general the objective decreases more quickly when eigenvalues form a small number of tight clusters (Stiefel, 1958; Kaniel, 1966; Nocedal & Wright, 2006).

A key appealing property of CG methods stems from the ability to generate descent directions satisfying the conjugacy property by considering only the last descent direction rather than all past descent directions. In particular, by taking $\mathbf{p}^0 = -\nabla f(\mathbf{x}^0)$ and $\mathbf{p}^{k+1} \leftarrow -\nabla f(\mathbf{x}^k) + \beta_k \mathbf{p}^k$ where $\beta_k = \|\nabla f(\mathbf{x}^k)\|^2 / \|\nabla f(\mathbf{x}^{k-1})\|^2$, one can ensure conjugacy for quadratics given exact line search, i.e., optimal α . Hence, the algorithm does not require storing a long history of past descent directions or Hessian approximations. We refer the reader to Algorithm 5.2 of Nocedal & Wright (2006) for further details. Fletcher & Reeves (1964) made the important observation that virtually the same algorithm can be used to minimize general non-linear objectives and without requiring exact line search. It was shown by Zoutendijk (1970) that the Fletcher-Reeves (FR) method converges with exact line search. Later, Al-Baali (1985) provided convergence results under certain assumptions on the objective function and an inexact line search. However, the FR method is known to produce unproductive descent directions with a small angle between them in some cases, thereby slowing down convergence (Gilbert & Nocedal, 1992). This motivated a slew of different approaches to compute β_k (Nocedal & Wright, 2006). Of particular relevance to our efforts is the Polak-Ribiere (PR) method, which ameliorates the issue (Nocedal & Wright, 2006):

$$\beta_k^{PR} = \frac{\langle \nabla f(\mathbf{x}^k) - \nabla f(\mathbf{x}^{k-1}), \nabla f(\mathbf{x}^k) \rangle}{\|\nabla f(\mathbf{x}^{k-1})\|^2}. \quad (9 \text{ revisited})$$

As noted by Nocedal & Wright (2006), “nonlinear conjugate gradient methods possess surprising, sometimes bizarre, convergence properties”. Proofs of convergence are typically easier to obtain than are rates of convergence (see Ch. 3 of Andrei (2020) for such results). However, one practical way to improve the convergence rate of linear and non-linear CG (NCG) is via *preconditioning*. By making a change of variables $\mathbf{x} = S\hat{\mathbf{x}}$, one reduces the condition number of the problem and/or renders the eigenvalues of the reparametrized problem more tightly clustered relative to the original for improved convergence (ideally, $SS^\top \approx \nabla^2 f^{-1}$). For further details on CG methods, we refer the reader to the survey by Hager & Zhang (2006b).

A.4 Line Search

Given a descent direction $\mathbf{p}^k \in \mathbb{R}^n$, i.e., a direction that satisfies $\langle \mathbf{p}^k, \nabla f(\mathbf{x}^k) \rangle \leq 0$, line search algorithms aim to find an appropriate step size α , where $\mathbf{x}^{k+1} \leftarrow \mathbf{x}^k + \alpha \mathbf{p}^k$. Perhaps the most well-known of desirable properties that a step size α should satisfy at any given optimization step are the Wolfe conditions (Wolfe, 1969, 1971). Given $\phi(\alpha) := f(\mathbf{x}^k + \alpha \mathbf{p}^k)$:

$$\frac{\phi(\alpha) - \phi(0)}{\alpha} \leq c_1 \phi'(0) \quad (26a)$$

$$\phi'(\alpha) \geq c_2 \phi'(0). \quad (26b)$$

where $0 < c_1 < c_2 < 1$ and (26a) and (26b) are known as the *sufficient decrease* and *curvature* conditions respectively (Nocedal & Wright, 2006). It is well known that given step sizes satisfying the Wolfe conditions and descent directions \mathbf{p}^k that are *not* nearly orthogonal to the steepest descent directions $-\nabla f(\mathbf{x}^k)$, line search methods ensure convergence of the gradient norms to zero (Zoutendijk, 1966; Wolfe, 1969, 1971). Instead of satisfying (26), some algorithms or theoretical analyses consider *exact* line search, where $\alpha^* \in \arg \min_{\alpha \in \mathbb{R}} \phi(\alpha)$, which clearly has a unique closed-form solution for quadratic objectives with a positive definite Hessian. However, a rule of thumb for general non-linear objectives is to not spend too much time finding α^* (Nocedal & Wright, 2006).

Hager & Zhang (2006a) proposed *approximate* Wolfe conditions, derived by replacing the $\phi(\alpha)$ and $\phi(0)$ terms in (26a) with $q(\alpha)$ and $q(0)$, where q is a quadratic interpolant of ϕ such that $q(0) = \phi(0)$, $q'(0) = \phi'(0)$ and $q'(\alpha) = \phi'(\alpha)$:

$$(2c_1 - 1)\phi'(0) \geq \phi'(\alpha) \geq c_2 \phi'(0). \quad (27)$$

A key advantage of replacing (26) by (27) stems from the fact that one only needs to evaluate ϕ' rather than both ϕ and ϕ' to check whether the conditions are satisfied, thereby halving the amount of computation necessary per iteration in cases where their evaluation has similar computational cost.

Bisection is a simple line search strategy with convergence guarantees particularly when the objective (and, therefore ϕ) is convex. One simply maintains a bracket $[\alpha_{\text{lo}}, \alpha_{\text{hi}}]$, where $\phi'(\alpha_{\text{lo}}) < 0$ and $\phi'(\alpha_{\text{hi}}) > 0$, and recursively considers their average and updates either endpoint of the bracket given the sign of $\phi'((\alpha_{\text{hi}} + \alpha_{\text{lo}})/2)$. Inspired by [Hager & Zhang \(2006a\)](#), we use a hybrid approach using bisection and the secant method (further details in Appx. C) to find α that satisfy (27) efficiently.

B Proofs and Additional Results

Lemma A.1 (A mirror descent bound for linear objectives). *Given a linear objective function $f(\mathbf{x}) = \langle \mathbf{x}, \mathbf{w} \rangle$, an initial point $\mathbf{x}^0 \in \mathcal{F}$, an optimal point \mathbf{x}^* and any $T > 0$, a sequence $[\mathbf{x}^t]_{t \in \mathbb{N}}$ obtained via (5) satisfies:*

$$f(\mathbf{x}^T) - f(\mathbf{x}^*) \leq \frac{D_h(\mathbf{x}^* | \mathbf{x}^0)}{\sum_{t=0}^{T-1} \gamma_t}. \quad (25)$$

Proof. For any $\mathbf{x} \in \mathcal{D}$,

$$\begin{aligned} f(\mathbf{x}^{t+1}) - f(\mathbf{x}) &= \langle \nabla f(\mathbf{x}^t), \mathbf{x}^{t+1} - \mathbf{x} \rangle && \text{(since } f \text{ is linear)} \\ &= \frac{1}{\gamma_t} \langle \nabla h(\mathbf{x}^t) - \nabla h(\hat{\mathbf{x}}^{t+1}), \mathbf{x}^{t+1} - \mathbf{x} \rangle && \text{(due to (7))} \\ &\leq \frac{1}{\gamma_t} \langle \nabla h(\mathbf{x}^t) - \nabla h(\mathbf{x}^{t+1}), \mathbf{x}^{t+1} - \mathbf{x} \rangle && \text{(by Lemma 4.1 in Bubeck (2015))} \\ &= \frac{1}{\gamma_t} (D_h(\mathbf{x} | \mathbf{x}^t) - D_h(\mathbf{x} | \mathbf{x}^{t+1}) - D_h(\mathbf{x}^{t+1} | \mathbf{x}^t)) && \text{(by Eq. 4.1 in Bubeck (2015))} \\ &\leq \frac{1}{\gamma_t} (D_h(\mathbf{x} | \mathbf{x}^t) - D_h(\mathbf{x} | \mathbf{x}^{t+1})), && \text{(since } D_h \geq 0 \text{)} \end{aligned}$$

which implies

$$\gamma_t (f(\mathbf{x}^{t+1}) - f(\mathbf{x})) \leq D_h(\mathbf{x} | \mathbf{x}^t) - D_h(\mathbf{x} | \mathbf{x}^{t+1}).$$

The above inequality proves monotonic improvement in each step t once we take $\mathbf{x} = \mathbf{x}^t$. Letting $\mathbf{x} = \mathbf{x}^*$, taking a telescopic sum and dividing both sides by $\bar{\gamma} = \sum_{s=0}^{T-1} \gamma_s$ we arrive at :

$$\begin{aligned} \frac{1}{\bar{\gamma}} \sum_{t=0}^{T-1} \gamma_t f(\mathbf{x}^{t+1}) - f(\mathbf{x}^*) &\leq \frac{D_h(\mathbf{x}^* | \mathbf{x}^0) - D_h(\mathbf{x}^* | \mathbf{x}^T)}{\bar{\gamma}} \\ &\leq \frac{D_h(\mathbf{x}^* | \mathbf{x}^0)}{\bar{\gamma}}, \end{aligned}$$

which implies (25) since improvement is monotonic and the first term on the LHS is a convex combination of objective values. \blacksquare

Lemma 3.1. *Given $h(P) = \sum_{ij} P_{ij} \log P_{ij}$ and $P^t, P^{t+1} \in \mathcal{U}(\mathbf{r}, \mathbf{c})$ related via (10), we have*

$$\langle P^t, C \rangle - \langle P^{t+1}, C \rangle = \frac{1}{\gamma_t} (D_{\text{KL}}(P^t | P^{t+1}) + D_{\text{KL}}(P^{t+1} | P^t)). \quad (11)$$

Proof. The proof of the equality follows similarly to the proof of Lemma A.1, except the first inequality is replaced with a strict equality in the special case that the feasible set $\mathcal{F} = \mathcal{U}(\mathbf{r}, \mathbf{c})$ and

$$h(P) = \sum_{ij} P_{ij} \log P_{ij}.$$

$$\begin{aligned}
& \langle P^t, C \rangle - \langle P^{t+1}, C \rangle \\
&= \langle \nabla f(P^t), P^t - P^{t+1} \rangle && \text{(since } f \text{ is linear)} \\
&= \frac{1}{\gamma} \langle \nabla h(P^t) - \nabla h(\hat{P}^{t+1}), P^t - P^{t+1} \rangle && \text{(due to (7))} \\
&= \frac{1}{\gamma} \langle \nabla h(P^t) - \nabla h(P^{t+1}), P^t - P^{t+1} \rangle && \text{(see below)} \\
&= \frac{1}{\gamma} (D_h(P^t, P^{t+1}) + D_h(P^{t+1}, P^t)). && \text{(by definition of the Bregman divergence as in (6))}
\end{aligned}$$

To see why the second last equality holds, note that $\nabla h(P)_{ij} = 1 + \log P_{ij}$ and $P_{ij}^{t+1} = \hat{P}_{ij}^{t+1} \exp\{u_i^* + v_j^*\}$. Then, for any $P, P' \in \mathcal{U}(\mathbf{r}, \mathbf{c})$,

$$\begin{aligned}
& \langle \nabla h(P^{t+1}), P - P' \rangle \\
&= \sum_{ij} (1 + \log \hat{P}_{ij}^{t+1} + u_i^* + v_j^*) (P_{ij} - P'_{ij}) \\
&= \langle \nabla h(\hat{P}^{t+1}), P - P' \rangle + \sum_i u_i^* \sum_j (P_{ij} - P'_{ij}) + \sum_j v_j^* \sum_i (P_{ij} - P'_{ij}) \\
&= \langle \nabla h(\hat{P}^{t+1}), P - P' \rangle + \langle \mathbf{u}^*, \mathbf{r} - \mathbf{r}' \rangle + \langle \mathbf{v}^*, \mathbf{c} - \mathbf{c}' \rangle && \text{(since } P, P' \in \mathcal{U}(\mathbf{r}, \mathbf{c}) \text{ by construction)} \\
&= \langle \nabla h(\hat{P}^{t+1}), P - P' \rangle.
\end{aligned}$$

■

Proposition 3.2 (Mirror descent error bounds for optimal transport). *Let $[\gamma_t]_{t=0}^{T-1}$ be a sequence of step sizes with $\sum_{t=0}^{T-1} \gamma_t = \bar{\gamma}$. Given a plan P^0 followed by a sequence of T plans computed via (10):*

$$\langle P^T, C \rangle - \langle P^*, C \rangle \leq \frac{D_h(P^* | P^0)}{\bar{\gamma}}. \quad (12)$$

Furthermore, let $H_{\min} = \min(H(\mathbf{r}), H(\mathbf{c}))$. If $h(\mathbf{x}) = \sum_i x_i \log x_i$ and $P^0 = \mathbf{r}\mathbf{c}^\top$:

$$\langle P^T, C \rangle - \langle P^*, C \rangle \leq \frac{H_{\min}}{\bar{\gamma}}. \quad (13)$$

Proof. (12) follows from Lemma A.1 since the OT objective $f(P)$ is linear. We turn our attention to (13). Recall that for $h(\mathbf{x}) = \sum_i x_i \log x_i$, we have $D_h(\mathbf{x} | \mathbf{y}) = D_{\text{KL}}(\mathbf{x} | \mathbf{y})$ on the simplex.

$$\begin{aligned}
D_{\text{KL}}(P^* | P^0) &= \sum_{ij} P_{ij}^* (\log P_{ij}^* - \log r_i c_j) \\
&= \sum_{ij} P_{ij}^* (\log P_{ij}^* - \log r_i - \log c_j) \\
&= -H(P^*) - \sum_i \log r_i \sum_j P_{ij}^* - \sum_j \log c_j \sum_i P_{ij}^* \\
&= -H(P^*) - \sum_i r_i \log r_i - \sum_j c_j \log c_j && \text{(since } P^* \in \mathcal{U}(\mathbf{r}, \mathbf{c})\text{)} \\
&= H(\mathbf{r}) + H(\mathbf{c}) - H(P^*) \\
&= \max(H(\mathbf{r}), H(\mathbf{c})) + \min(H(\mathbf{r}), H(\mathbf{c})) - H(P^*) \\
&\leq \min(H(\mathbf{r}), H(\mathbf{c})).
\end{aligned}$$

The last inequality holds since $H(P) \geq H(\mathbf{r})$ and $H(P) \geq H(\mathbf{c})$ for any $P \in \mathcal{U}(\mathbf{r}, \mathbf{c})$ (Cover & Thomas, 2006), which together imply $H(P) \geq \max(H(\mathbf{r}), H(\mathbf{c}))$. ■

Lemma 3.3. *Let $P_1, P_2 \in \mathcal{U}(\mathbf{r}, \mathbf{c})$ be computed over T_1 and T_2 steps of MD with arbitrary schedules γ_t such that the sum of MD step sizes equal $\bar{\gamma}$ for both given any initial plan $P^0 \in \mathbb{R}_{>0}^{n \times n}$ of rank 1. Further, let P_3 be the solution of problem (2) with $\gamma = \bar{\gamma}$. We have $P_1 = P_2 = P_3$.*

Proof. Recall that any rank 1 matrix can be written as an outer product of two vectors. Suppose P^0 equals $\mathbf{r}_1 \mathbf{c}_1^\top$ for the first MD procedure and $\mathbf{r}_2 \mathbf{c}_2^\top$ for the second. Now, write the optimal sequence of dual variables over MD steps for the two MD procedures as $(\mathbf{u}_1^t, \mathbf{v}_1^t)$ and $(\mathbf{u}_2^t, \mathbf{v}_2^t)$. At step T_1 ,

$$\begin{aligned} P_1 &= P^0 \odot \exp \left\{ \sum_{t \leq T_1} \mathbf{u}_1^t \mathbf{1}_n^\top + \mathbf{1}_n \sum_{t \leq T_1} (\mathbf{v}_1^t)^\top - \sum_{t \leq T_1} \gamma_t C \right\} \\ &= \exp \left\{ \left(\log \mathbf{r}_1 + \sum_{t \leq T_1} \mathbf{u}_1^t \right) \mathbf{1}_n^\top + \mathbf{1}_n \left(\log \mathbf{c}_1 + \sum_{t \leq T_1} (\mathbf{v}_1^t) \right)^\top - \bar{\gamma} C \right\}, \end{aligned}$$

and similarly,

$$P_2 = \exp \left\{ \left(\log \mathbf{r}_2 + \sum_{t \leq T_2} \mathbf{u}_2^t \right) \mathbf{1}_n^\top + \mathbf{1}_n \left(\log \mathbf{c}_2 + \sum_{t \leq T_2} (\mathbf{v}_2^t) \right)^\top - \bar{\gamma} C \right\}.$$

Since both $P_1, P_2 \in \mathcal{U}(\mathbf{r}, \mathbf{c})$ and the projection of $\exp\{-\bar{\gamma}C\}$ onto $\mathcal{U}(\mathbf{r}, \mathbf{c})$ is unique by the strict convexity of the Lagrangian dual (see (3)), we conclude that $P_1 = P_2$ with a simple reparametrization $\log \mathbf{r}_1 + \sum_{t \leq T_1} \mathbf{u}_1^t + \delta = \log \mathbf{r}_2 + \sum_{t \leq T_2} \mathbf{u}_2^t$ and $\log \mathbf{c}_1 + \sum_{t \leq T_1} \mathbf{v}_1^t - \delta = \log \mathbf{c}_2 + \sum_{t \leq T_2} \mathbf{v}_2^t$ for some $\delta \in \mathbb{R}$. Entropy-regularized OT problem is only a special case where $P^0 = \mathbf{1}_n \mathbf{1}_n^\top$ and $T = 1, \gamma_t = \bar{\gamma}$. ■

Corollary 3.4. *Given the same setting as Lemma 3.1,*

$$\|P^{t+1} - P^t\|_1 \leq \min \left(\gamma_t, \sqrt{\frac{H_{\min} \gamma_t}{\sum_t \gamma_t}} \right). \quad (16)$$

Proof. First, recall Pinsker's inequality for distributions $\mathbf{x}, \mathbf{y} \in \Delta_n$:

$$\frac{1}{2} \|\mathbf{x} - \mathbf{y}\|_1^2 \leq D_{\text{KL}}(\mathbf{x} \|\mathbf{y}).$$

Applying Pinsker's inequality to (11):

$$\begin{aligned} \frac{1}{\gamma_t} \|P^t - P^{t+1}\|_1^2 &\leq \langle P^t - P^{t+1}, C \rangle \\ &\Rightarrow \frac{1}{\gamma_t} \|P^t - P^{t+1}\|_1^2 \leq \|P^t - P^{t+1}\|_1 \|C\|_\infty && \text{(by Hölder's inequality)} \\ &\Rightarrow \|P^t - P^{t+1}\|_1 \leq \gamma_t. && \text{(since } \|C\|_\infty \leq 1 \text{ by construction)} \end{aligned}$$

Now, we show the second inequality:

$$\begin{aligned} \langle P^t - P^*, C \rangle &\leq \frac{H_{\min}}{\sum_t \gamma_t} && \text{(Proposition 3.2)} \\ \Rightarrow \langle P^t - P^{t+1}, C \rangle &\leq \frac{H_{\min}}{\sum_t \gamma_t} - \langle P^{t+1} - P^*, C \rangle \leq \frac{H_{\min}}{\sum_t \gamma_t} && \text{(since } P^* \text{ is optimal)} \\ \Rightarrow \frac{1}{\gamma_t} (D_{\text{KL}}(P^t \| P^{t+1}) + D_{\text{KL}}(P^{t+1} \| P^t)) &\leq \frac{H_{\min}}{\sum_t \gamma_t} && \text{(by Lemma 3.1)} \\ \Rightarrow \|P^t - P^{t+1}\|_1^2 &\leq \frac{H_{\min} \gamma_t}{\sum_t \gamma_t} && \text{(by Pinsker's inequality)} \\ \Rightarrow \|P^t - P^{t+1}\|_1 &\leq \sqrt{\frac{H_{\min} \gamma_t}{\sum_t \gamma_t}}. && \end{aligned}$$

■

Proposition B.1. Let $\|\mathbf{x}\|_{\text{var}} := \max_i x_i - \min_i x_i$ and Hilbert's projective metric be given by $D_{\text{HP}}(\mathbf{p}, \mathbf{q}) := \|\log(\mathbf{p}/\mathbf{q})\|_{\text{var}}$, where $\mathbf{p}, \mathbf{q} \in \mathbb{R}_{>0}^m$. Let $P^{t,k}$ denote the k^{th} Sinkhorn projection iterate at the t^{th} MD time-step under a fixed step size γ . Given $\kappa_t := \tanh\left(\frac{\gamma t \|C\|_\infty}{2}\right)$, $\bar{\kappa}_t(k) := \frac{\kappa_t^k}{1-\kappa_t^2}$, for any $k \geq 1$ and $t \geq 1$,

$$D_{\text{HP}}(P^{t,k}, P^t) \leq \bar{\kappa}_t(k) (D_{\text{HP}}(\mathbf{r}(P^{t,0}), \mathbf{r}) + D_{\text{HP}}(\mathbf{c}(P^{t,0}), \mathbf{c})). \quad (28)$$

Proof. Recall from [Franklin & Lorenz \(1989\)](#) that given a sequence of Sinkhorn iterates $A^k = \mathbf{D}(\mathbf{x}^k)A^0\mathbf{D}(\mathbf{y}^k)$ for $\mathbf{x}^k, \mathbf{y}^k \in \mathbb{R}_{++}^n$ with $\mathbf{x}^0 = \mathbf{y}^0 = \mathbf{1}_n$,

$$\hat{D}(A^k, A^*) \leq \frac{\kappa(G)^k}{1 - \kappa(G)^2} (D_{\text{HP}}(\mathbf{r}(A^0), \mathbf{r}) + D_{\text{HP}}(\mathbf{c}(A^0), \mathbf{c})), \quad (29)$$

where the following re-express the definitions from [Franklin & Lorenz \(1989\)](#) necessary to parse (29) and our proof steps that follow:

1. G is any matrix that is *diagonally equivalent* to A^* , i.e., $G \sim A^*$ if there exist $\mathbf{x}', \mathbf{y}' \in \mathbb{R}_{++}^n$ such that $G = \mathbf{D}(\mathbf{x}')A^*\mathbf{D}(\mathbf{y}')$.
2. $\hat{D}(A, B) := D_{\text{HP}}(\mathbf{x}, \mathbf{1}_n) + D_{\text{HP}}(\mathbf{y}, \mathbf{1}_n)$ for $A = \mathbf{D}(\mathbf{x})B\mathbf{D}(\mathbf{y})$. \hat{D} is a metric over the set of diagonally equivalent matrices of which A and B are elements.
3. $\kappa(G)$ is called the contraction ratio of G and is given by the following:

$$\kappa(G) := \frac{\sqrt{\nu(G)} - 1}{\sqrt{\nu(G)} + 1},$$

where $\nu(G) = \max_{i,j,k,l} \frac{G_{ik}G_{jl}}{G_{jk}G_{il}}$ is called the diameter of G 's image. Any two matrices $G \sim G'$ have the same contraction ratio as diagonal terms contributing to $\nu(\mathbf{D}(\mathbf{x})G\mathbf{D}(\mathbf{y}))$ cancel out.

4. $A^* \in \mathcal{U}(\mathbf{r}, \mathbf{c})$ is diagonally equivalent to A^0 .

In our case, A^* in (29) corresponds to the exact MD iterate $P^t = \mathbf{D}(\exp\{\mathbf{u}^*\})P^{t,0}\mathbf{D}(\exp\{\mathbf{v}^*\})$ at time t , while A^k corresponds to $P^{t,k} = \mathbf{D}(\exp\{\mathbf{u}^k\})P^{t,0}\mathbf{D}(\exp\{\mathbf{v}^k\})$. That is,

$$P^t = \mathbf{D}(\exp\{\mathbf{u}^* - \mathbf{u}^k\})P^{t,k}\mathbf{D}(\exp\{\mathbf{v}^* - \mathbf{v}^k\})$$

Hence, given the definition of \hat{D} :

$$\begin{aligned} \hat{D}(P^{t,k}, P^t) &= D_{\text{HP}}(\exp\{\mathbf{u}^* - \mathbf{u}^k\}, \mathbf{1}_n) + D_{\text{HP}}(\exp\{\mathbf{v}^* - \mathbf{v}^k\}, \mathbf{1}_n) \\ &= \|\mathbf{u}^* - \mathbf{u}^k\|_{\text{var}} + \|\mathbf{v}^* - \mathbf{v}^k\|_{\text{var}} \\ &= \|\mathbf{u}^* \mathbf{1}^\top + \mathbf{1}(\mathbf{v}^*)^\top - \mathbf{u}^k \mathbf{1}^\top - \mathbf{1}(\mathbf{v}^k)^\top\|_{\text{var}} \\ &= \|\mathbf{u}^* \mathbf{1}^\top + \mathbf{1}(\mathbf{v}^*)^\top - \gamma C - \mathbf{u}^k \mathbf{1}^\top - \mathbf{1}(\mathbf{v}^k)^\top + \gamma C\|_{\text{var}} \\ &= \left\| \log \left(\frac{K(\mathbf{u}^*, \mathbf{v}^*)}{K(\mathbf{u}^k, \mathbf{v}^k)} \right) \right\|_{\text{var}} \\ &= \left\| \log \left(\frac{P^{t,0} \odot K(\mathbf{u}^*, \mathbf{v}^*)}{P^{t,0} \odot K(\mathbf{u}^k, \mathbf{v}^k)} \right) \right\|_{\text{var}} \\ &= D_{\text{HP}}(P^{t,k}, P^t), \end{aligned}$$

which proves the equality in (28). Now, we show that the contraction ratio of the matrices $P^{t,k}$ at time t are bounded above by κ_t , which will conclude the proof of (28). Since $P^t \sim P^{t,k} \sim P^{t,k'}$ for any $k, k' \geq 0$, we can show the contraction ratio for any matrix that is diagonally equivalent to P^t , which can be written as:

$$\begin{aligned} P^t &= \mathbf{D}(\exp\{\bar{\mathbf{u}}^*\})(\mathbf{r}\mathbf{c}^\top \odot \exp\{-\gamma t C\})\mathbf{D}(\exp\{\bar{\mathbf{v}}^*\}) \\ &= \mathbf{D}(\mathbf{r} \odot \exp\{\bar{\mathbf{u}}^*\}) \exp\{-\gamma t C\} \mathbf{D}(\mathbf{c} \odot \exp\{\bar{\mathbf{v}}^*\}). \end{aligned}$$

Hence, all $P^{t,k}$ are diagonally equivalent to $\exp\{-\gamma t C\}$. The diameter of the image is:

$$\begin{aligned}\nu(\exp\{-\gamma t C\}) &= \max_{i,j,k,l} \exp\{-\gamma t(C_{ik} + C_{jl} - C_{jk} - C_{il})\} \\ &= \exp\{\gamma t \max_{i,j,k,l} (C_{ik} + C_{jl} - C_{jk} - C_{il})\} \\ &\leq \exp\{2\gamma t \|C\|_\infty\}. \quad (\text{since } C_{ij} \geq 0 \text{ for all } i, j \text{ by construction})\end{aligned}$$

Since κ is monotone-increasing in ν , this implies

$$\kappa(\exp\{-\gamma t C\}) \leq \frac{\exp\{\gamma t \|C\|_\infty\} - 1}{\exp\{\gamma t \|C\|_\infty\} + 1} = \tanh\left(\frac{\gamma t \|C\|_\infty}{2}\right) = \kappa_t. \quad \blacksquare$$

C An Efficient Line Search Algorithm

To perform line search for the preconditioned NCG (PNCG) approach, we adopt a hybrid strategy combining bisection and the secant method to find α_k that satisfies approximate Wolfe conditions (27). Given $\alpha_{\text{lo}}, \alpha_{\text{hi}}$, the secant method computes the minimizer of a quadratic interpolant \hat{q} that satisfies $\hat{q}'(\alpha_{\text{lo}}) = \phi'(\alpha_{\text{lo}})$ and $\hat{q}'(\alpha_{\text{hi}}) = \phi'(\alpha_{\text{hi}})$ as follows:

$$\alpha_{\text{sec}} = \frac{\alpha_{\text{lo}}\phi'(\alpha_{\text{hi}}) - \alpha_{\text{hi}}\phi'(\alpha_{\text{lo}})}{\phi'(\alpha_{\text{hi}}) - \phi'(\alpha_{\text{lo}})}, \quad (30)$$

where evaluation of ϕ' has computational complexity $O(n^2)$ as does a single step of SA:

$$\phi'(\alpha) = \langle \mathbf{p}_u \mathbf{1}^\top + \mathbf{1} \mathbf{p}_v^\top, P(\alpha) \rangle - \langle \mathbf{p}_u, \mathbf{r} \rangle - \langle \mathbf{p}_v, \mathbf{c} \rangle. \quad (31)$$

In our case, the objective is convex and we ensure $\phi'(\alpha_{\text{lo}}) < 0$ and $\phi'(\alpha_{\text{hi}}) > 0$ so that we are guaranteed to have $\alpha_{\text{lo}} < \alpha_{\text{sec}} < \alpha_{\text{hi}}$. Thus, the updated bracket is guaranteed to be smaller once we replace either of α_{lo} or α_{hi} by α_{sec} for the next bracket given the sign of $\phi'(\alpha_{\text{sec}})$. If ϕ behaves like a quadratic inside the bracket, the secant method converges very quickly, but convergence can be arbitrarily slow otherwise. For this reason, we simply average the bisection estimate and α_{sec} for a less aggressive but more reliable line search that still converges quickly, i.e., $\alpha_{\text{hybrid}} = 0.5\alpha_{\text{sec}} + 0.5(\alpha_{\text{hi}} + \alpha_{\text{lo}})/2$. In our experiments, we find that the average number of ϕ' evaluations necessary to find an α that satisfies (27) is typically between 2 – 4. While the approach outlined here is extremely easy to implement (including as a batch process) and works well in practice, other line search procedures at the pareto-frontier of the efficiency-precision plane may benefit Alg. 2.

D Related Work

The linear program (LP) form of the original optimal transport problem given by (1) can be solved via any LP solver including those based on interior-point methods and the simplex method (see Chapters 13 and 14 of [Nocedal & Wright \(2006\)](#) respectively). While problem (1) is a special case of LPs, it has received significant attention from the optimization community owing to its equivalence to an important class of LPs called the minimum-cost-flow problems ([Peyré et al., 2019](#)). Specialized interior-point methods can compute exact solutions in $\tilde{O}(n^{5/2})$ time ([Lee & Sidford, 2014](#)). A randomized interior-point algorithm recently proposed by [van den Brand et al. \(2021\)](#) achieves a complexity bound of $\tilde{O}(n^2)$, but the feasibility of its scalable implementation has been brought to question ([Lin et al., 2022](#)). Similar to interior-point methods, specialized simplex methods called network simplex algorithms can find exact solutions with better complexity than their naive counterparts. For example, the algorithm presented by [Orlin \(1997\)](#) can find exact solutions in $\tilde{O}(n^3)$ time. [Lahn et al. \(2019\)](#) developed a faster algorithm that can compute transport plans with arbitrary accuracy without encountering numerical instabilities and was shown to be competitive with SA in the sequential setting; however, the question of parallel implementation was left open.

More closely related to our work, entropic regularization of OT has gained significant attention by the machine learning community since the work of [Cuturi \(2013\)](#) perhaps owing to the simplicity of

SA and its GPU-friendliness, as well as sample complexity benefits of entropic regularization in the continuous setting (Genevay et al., 2019). Altschuler et al. (2017) proved $\tilde{\mathcal{O}}(n^2\varepsilon^{-3})$ computational complexity for SA, where $\varepsilon = \langle P - P^*, C \rangle$. Dvurechensky et al. (2018) improved upon this bound and proved $\tilde{\mathcal{O}}(n^2\varepsilon^{-2})$. Both papers also proposed new algorithms. In particular, Altschuler et al. (2017) proposed the Greenkhorn algorithm, which greedily selects individual rows or columns to scale at a given step instead of scaling all rows or columns of iterates P at once as done in SA. While this was shown to converge more quickly than SA in terms of the number of row/column updates performed, practical speedup over GPU-parallel processing has not been demonstrated to the best of our knowledge. Regardless, Lin et al. (2019) proved a matching bound of $\tilde{\mathcal{O}}(n^2\varepsilon^{-2})$ for Greenkhorn. Dvurechensky et al. (2018) proposed an adaptive primal-dual accelerated gradient descent (APDAGD) algorithm with a complexity bound of $\tilde{\mathcal{O}}(n^{5/2}\varepsilon^{-1})$ refined by Lin et al. (2019). In the same paper, Lin et al. (2019) proposed an adaptive primal-dual accelerated *mirror* descent (APDAMD) algorithm with complexity $\tilde{\mathcal{O}}(n^2\sqrt{\delta}\varepsilon^{-1})$, where δ depends on the regularity of a chosen mirror map.

Empirical evaluations Lin et al. (2019) have shown that APDAMD outperforms APDAGD in terms of the number of iterations, but not SA. However these tests were done only in a high relative error setting ($> 50\%$) where the algorithms are shielded from possible numerical instabilities. Modest gains over SA in terms of number of iterations in the same regime were later obtained by Lin et al. (2022) (see their Figs. 1-2) via an accelerated alternating minimization (AAM) algorithm similar to that of Guminov et al. (2021), but with a slightly different trade-off between n and ε . Note that the APDAMD algorithm of Lin et al. (2019) applies MD to the regularized problem (2), while we consider its direct application to the original OT problem (1) in this work.

Application of MD to (1) has also been considered recently to approximately solve OT problems without running into numerical stability issues. While SA can be stabilized via implementation tricks involving log-domain computations, these can incur a substantial computational burden as noted in Sec. 4.4 of Peyré et al. (2019).

Yang & Toh (2022) discuss an algorithm similar to MDOT, although their approach differs from ours in a number of important aspects. First, they require a rounding procedure onto $\mathcal{U}(\mathbf{r}, \mathbf{c})$ after *each* MD iteration, as well as the verification of complicated stopping criteria for all Bregman projections, while we did not find these to be necessary for the OT problem in any of our experiments or mathematical considerations. Indeed, as shown in the proof of Lemma 3.3, the Bregman projection onto $\mathcal{U}(\mathbf{r}, \mathbf{c})$ of any matrices of the form $P \odot \exp\{-\bar{\gamma}(t)C\}$, where P is a rank-1 matrix, produces exactly the same transport plan such that there is no compounding of errors due to inexact Bregman projections. In fact, we argue that rounding the transport plan after each MD step could be a source of compounding errors, as rounding incurs error and the equivalence discussed in Lemma 3.3 is no longer guaranteed since the rank-1 property of P may be broken. Secondly, they only consider Sinkhorn projections, while we additionally introduce a more efficient projection algorithm (PNCG) to overcome the declining convergence rate of Sinkhorn iteration in MD. Lastly, we devoted special attention to the entropy of marginals, which yielded several insights regarding information-theoretic guarantees on ε , convergence speed and the feasibility of NCG for Bregman projections.

Also closely related is the Mirror Sinkhorn (MSK) algorithm of Ballu & Berthet (2022), which takes gradient steps in the dual space as in L5 of Alg. 1, but instead of subsequently performing an approximate projection onto $\mathcal{U}(\mathbf{r}, \mathbf{c})$, performs a single Sinkhorn update in an alternating fashion. Our empirical investigations suggested that this approach is only efficient in the high relative error regime (see Fig. 5). Xie et al. (2020) previously proposed an algorithm (IPOT) similar to MSK with a fixed, even number of Sinkhorn updates (usually 2) following gradient steps; we omitted additional empirical comparison to IPOT given its similarity with MSK.

E Additional Experiments

In Fig. 6, we repeat the experiments shown in Fig. 4 in the main text, except this time we fix $\varepsilon = 10^{-10}$ and vary the problem size $n \in \{2^8, 2^9, 2^{10}, 2^{11}, 2^{12}\}$. The experiments serve as a sanity check to ensure that the conjugate gradients approach does not suffer from a weaker dependence on n relative to Sinkhorn projections in practice. We do not observe any noticeable differences in the trends the number of iteration and wall-clock time curves follow with varying n . Notice also that the

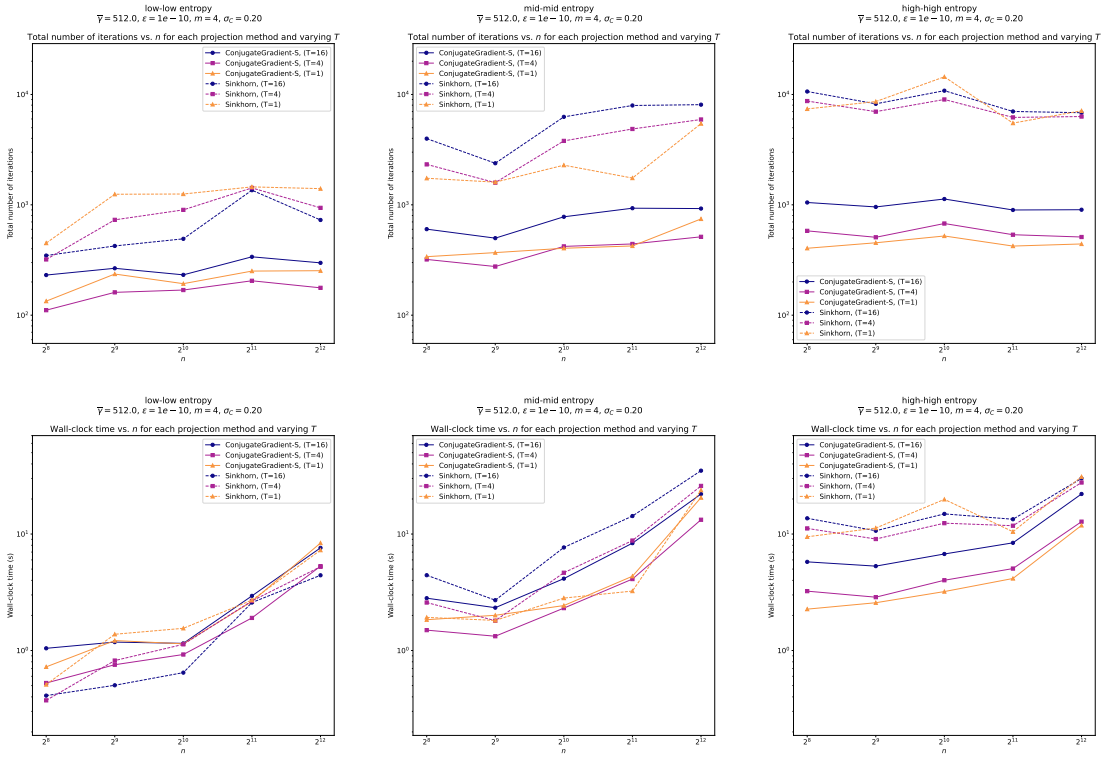


Figure 6: Number of iterations (**top**) and wall-clock time (**bottom**) vs. n for Sinkhorn and PNCG projections given $T \in \{1, 4, 16\}$ over $H(\mathbf{r})$ and $H(\mathbf{c})$ both approximately $\{0.1 \log_2 n, 0.5 \log_2, 0.9 \log_2 n\}$ and $\epsilon = 10^{-10}$ (**left-to-right**). Both methods appear to have similar dependence on n with no significant differences in trends for either number of iterations or wall-clock time.

total number of mirror descent steps T also does not seem to have an obvious dependence on n .